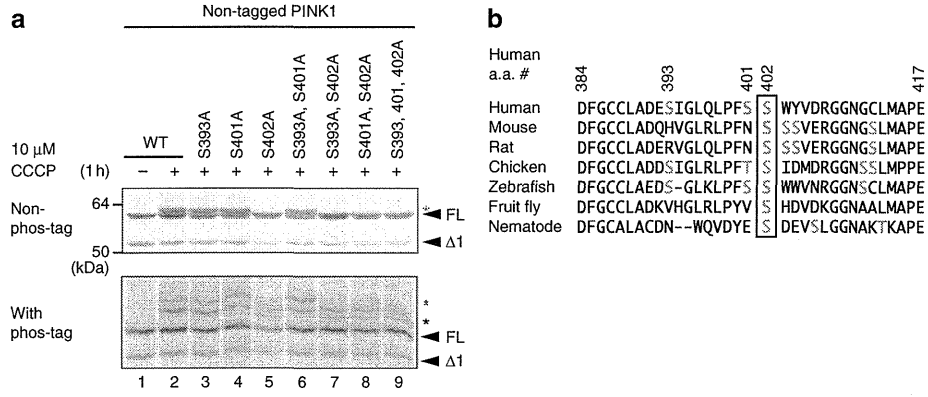

Figure 3 | S402A mutation partly inhibits the autophosphorylation of PINK1. (**a**) The S402A mutation altered the phosphorylation pattern of PINK1. PINK1 with the indicated mutations were transfected into HeLa cells and then subjected to SDS-PAGE on a 7.5% Tris-glycine gel ±50 μM phos-tag. Asterisks indicate phosphorylated PINK1 (see details of red and black asterisks in the text). (**b**) Ser/Thr residues in the activation loop of PINK1 from various organisms are shown in red font. Ser402 (boxed) is evolutionarily conserved.

(Fig. 2d). Next, PINK1-FLAG constructs harboring the various pathogenic mutations were transfected into HeLa cells with PINK1-GFP, treated with CCCP and then immunoblotted. As shown in Fig. 2e, while the majority of the mutants did not undergo phosphorylation in the presence of PINK1-GFP, a clear doublet was observed with the G409V PINK1 mutant (lane 8) and faint but reproducible doublet bands were also observed with the E240K and G386A mutants (lanes 4 and 7). Neither PINK1(G409V) alone nor co-expressed with PINK1(KD)-GFP underwent phosphorylation equivalent to WT PINK1 (lanes 4 and 6 of Fig. 2f). In contrast, PINK1(G409V) was clearly phosphorylated when WT PINK1-GFP was co-expressed (lane 5). These results suggest that autophosphorylation can occur *in trans* between two PINK1 molecules.

Ser228 and Ser402 are autophosphorylation sites of PINK1. We next sought to identify the PINK1 autophosphorylation site(s). As Ser/Thr residues in the activation loop of kinases are the most common and best-understood phosphorylation sites (for a review, see Huse and Kuriyan[42] and Nolen *et al.*[43]), we decided to focus on the PINK1 activation loop. In the case of PINK1, the region spanning amino-acid residues 384–417 (384DFG ... APE417) corresponds to the activation loop. Three Ser residues (Ser393, Ser401 and Ser402) are present within this region. We consequently exchanged these Ser residues for Ala. PINK1 with either the S393A or the S401A mutation still underwent phosphorylation in a manner similar to WT PINK1 (Fig. 3a, compare lanes 3 and 4 with lane 2). In contrast, the S402A mutation altered the band pattern of PINK1 (lane 5) with the upper band absent as assessed by conventional PAGE (non-phos-tag panel of Fig. 3a). The S402A mutation likewise affected the banding pattern on the phos-tag PAGE gel (phos-tag panel of Fig. 3a), with the emergence of a lower-molecular-weight band (black asterisk) slightly below the first band (red asterisk), which was absent in the mutation. Double and triple combinations of the S393A, S401A and S402A mutations failed to generate results that differed from the S402A mutation alone (lanes 7–9). The Ser residue at this position (402 in humans) is well conserved from mammals to nematodes, suggesting its physiological importance (Fig. 3b). The S402A mutation, however, did not impact all of the phosphorylation bands (Fig. 3a), suggesting that while S402 in the activation loop is dominantly phosphorylated, another PINK1 phosphorylation site is also utilized.

To identify the other phosphorylation site, we performed mass spectrometric analysis of autophosphorylated PINK1. Glutathione *S*-transferase (GST)-fused PINK1 was integrated into the genome of HEK293 cells by retrovirus-mediated transformation. PINK1-GST was then purified from this stable cell line following +/− CCCP treatment (Supplementary Fig. S2) and subjected to LC-MS/MS analysis after Asp-N protease digestion. A peptide equivalent to amino acids 206–230 (ERAPGAPAFPLAIKMMWNISAGSSS) was identified as a putative phosphorylated peptide. Although the unphosphorylated peptide was detected from both CCCP-treated and -untreated cells, the phosphorylated peptide was only detected from CCCP-treated cells (Fig. 4a). The MS/MS data suggested that Ser228, Ser229 or Ser230 was phosphorylated; more specific determination of the phosphorylation site is problematic (Fig. 4b). These candidate Ser residues have been relatively conserved during evolution (Fig. 4c). A peptide containing phospho-Ser402 was not identified in this analysis, possibly because the signal intensity was below the threshold of detection.

Although the three-dimensional structure of PINK1 has not yet been solved, a reliable structural model based on the structure of a related kinase (CaMKII) has been deposited in the Protein Model Database (accession code: PM0076345)[44]. Unexpectedly, we found that Ser228, Ser229 and Ser230 localized very close to Ser402 (Fig. 4d) and that they constituted a small structural patch on the surface of the PINK1 model (Supplementary Fig. S3). These Ser residues, as well as the spatially close Ser167 and Ser225, were serially exchanged for Ala. PINK1 with the S167A, S225A, S229A or S230A mutation showed double phosphorylated bands in phos-tag PAGE, although the molecular weight of those bands was altered to some degree (Fig. 4e). In contrast, the first band in phos-tag PAGE (red asterisk in Fig. 4e) disappeared in the S228A mutation (note that a faint band near the asterisk is a cross-reacting band also observed in lane 1 (WT)). Moreover, the PINK1 autophosphorylation signal was completely absent in the S228A/S402A double mutant (Fig. 4f, lane 4). Combining the S225A, S229A and S230A mutations with the S402A mutation had no such effect on the autophosphorylation signal (Fig. 4f, lanes 3, 5 and 6) and were almost indistinguishable from the S402A mutation alone (Fig. 3a, lanes 5). These results indicate that S228 and S402 are PINK1 autophosphorylation sites.

PINK1 autophosphorylation recruits Parkin to the mitochondria. Next, we sought to determine whether autophosphorylation of PINK1 is important to recruit Parkin to mitochondria. However, this experiment presents a unique challenge in that overexpression of exogenous PINK1 itself results in the targeting of Parkin to mitochondria irrespective of the mitochondrial $\Delta\Psi m$[7,45,46] and autophosphorylation (Fig. 1). We thus attempted to establish an

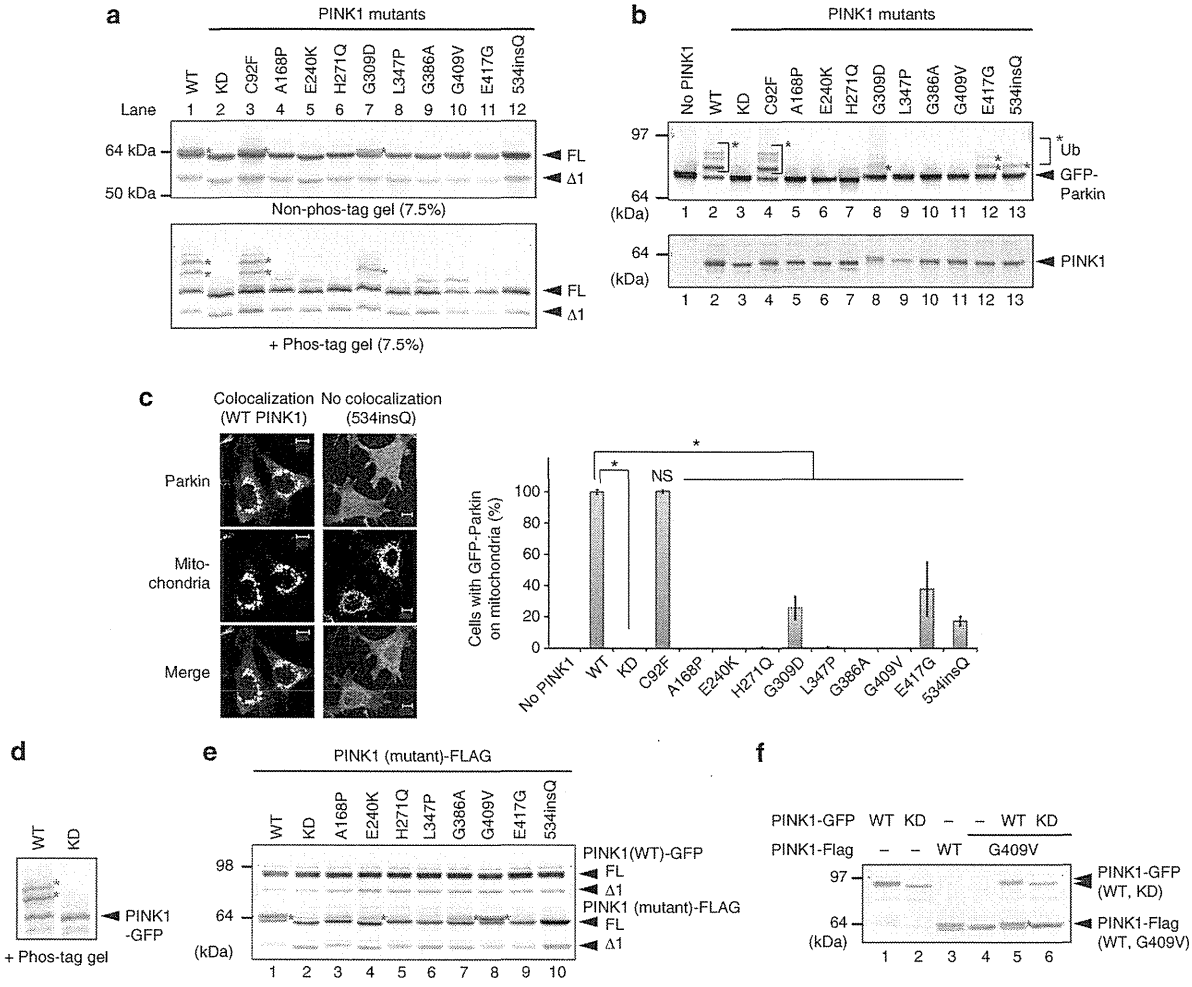

Figure 2 | PINK1 phosphorylation on damaged mitochondria is inhibited by most pathogenic mutations. (**a**) HeLa cells expressing PINK1-Flag with various pathogenic mutations were treated with CCCP, subjected to SDS-PAGE ± phos-tag and immunoblotted using an anti-PINK1 antibody. Red asterisks show phosphorylated PINK1. (**b**) *PINK1*$^{-/-}$ MEFs co-expressing GFP-Parkin and various pathogenic PINK1 mutants were subjected to non phos-tag PAGE and immunoblotting with anti-Parkin and anti-PINK1 antibodies. Blue asterisks show autoubiquitylation of GFP-Parkin, which is taken as evidence of its mitochondrial localization. (**c**) The subcellular localization of GFP-Parkin in *PINK1*$^{-/-}$ MEFs co-expressing various PINK1 mutants. Example figures indicative of colocalization and no colocalization are shown (bars, 10 μm). The number of cells with Parkin-positive mitochondria in the Parkin-expressing cells was counted in >100 cells. Error bars represent the mean±s.d. values of three experiments. Statistical significance was calculated using analysis of variance with a Tukey–Kramer *post hoc* test; *$P<0.01$; ns, not significant. (**d**) PINK1-GFP undergoes auto-phosphorylation following CCCP treatment. Red asterisks show the phosphorylated PINK1-GFP. (**e**) Various pathogenic PINK1 mutants were co-transfected with PINK1(WT)-GFP, treated with CCCP and subjected to immunoblotting using an anti-PINK1 antibody. Red asterisks show the phosphorylated bands. (**f**) HeLa cells expressing PINK1(G409V)-Flag with PINK1-GFP or PINK1(KD)-GFP were treated with CCCP and subjected to conventional PAGE. Red asterisks show phosphorylated PINK1(G409V)-Flag. FL, Δ1 and KD represent full-length PINK1, N-terminal processed PINK1 and KD mutant, respectively.

of GFP-Parkin when the aforementioned *PINK1* mutants were co-expressed in cells. We previously reported that the latent E3 activity of Parkin is activated upon recruitment to damaged mitochondria; as a consequence, autoubiquitylation of GFP-Parkin would be expected to be a good index of its mitochondrial localization[6]. In *PINK1*$^{-/-}$ MEFs co-expressing the various PINK1 mutants, only the C92F mutant exhibited autoubiquitylation of GFP-Parkin equivalent to WT PINK1 (Fig. 2b, lane 4). The G309D, E417G and 534insQ mutants showed weakened autoubiquitylation (lanes 8, 12 and 13). In contrast, the other PINK1 mutations severely hindered ubiquitylation of GFP-Parkin. Immunoblots confirmed that these mutants were expressed (Fig. 2b). Immunocytochemistry also confirmed the above results. Statistical analysis showed that co-expression of the C92F mutant resulted in the mitochondrial localization of GFP-Parkin, whereas the G309D, E417G and 534insQ mutants were unable to fully promote the mitochondrial localization of Parkin and the other pathogenic mutations failed to recruit GFP-Parkin to the mitochondria (Fig. 2c). These results showed that most pathogenic mutations compromised both the autophosphorylation activity of PINK1 and mitochondrial localization of Parkin.

We next analysed the mode of PINK1 phosphorylation. As the activity of many kinases is regulated by intermolecular interactions[41], we examined if the auto-phosphorylation of mutant PINK1 is ameliorated by co-expression with WT PINK1. When C-terminal GFP-tagged PINK1 (hereafter referred to as PINK1-GFP) was treated with CCCP and subjected to immunoblotting in the presence of phos-tag, slower-migrating phosphorylated bands were observed. These bands disappeared in the KD mutant, confirming that PINK1-GFP is functional and undergoes auto-phosphorylation

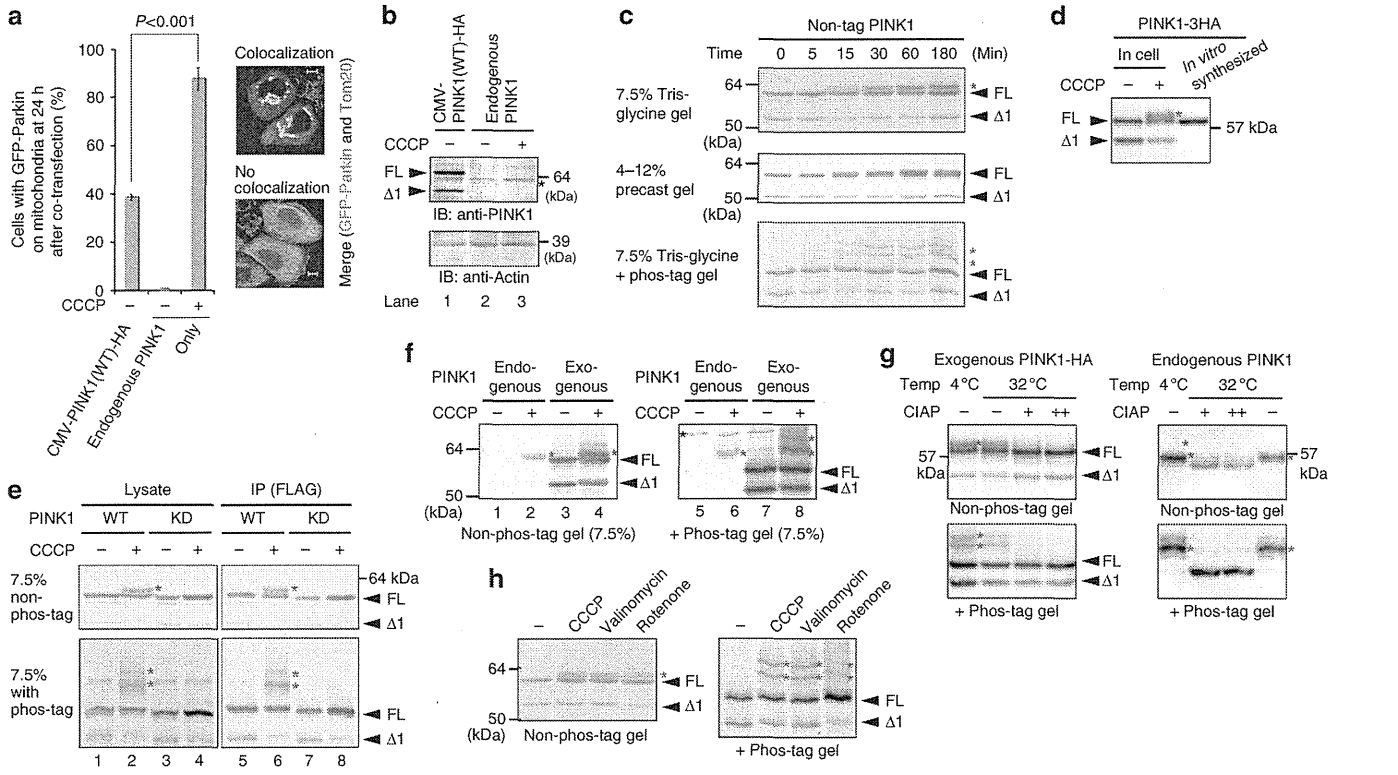

Figure 1 | PINK1 is phosphorylated following a decrease in mitochondrial $\Delta\Psi$m. (**a**) Endogenous PINK1 in the presence of CCCP (10 μM, 1 h) recruits Parkin to mitochondria more efficiently than over-produced PINK1 (CMV promoter-driven) in the absence of CCCP. The number of cells with Parkin-positive mitochondria in the Parkin-expressing cells was counted in >100 cells. Error bars represent the mean±s.d. values of three experiments. Statistical significance was calculated using analysis of variance with a Tukey–Kramer *post hoc* test. Example figures indicative of colocalization and no colocalization are shown on the right (scale bars, 10 μm). (**b**) Immunoblotting of exogenous and endogenous PINK1. The asterisk indicates the position of endogenous PINK1. Actin was used as a loading control. FL, full-length PINK1; Δ1, the N-terminal processed form. (**c**) HeLa cells expressing non-tagged PINK1 were treated with 10 μM CCCP for the indicated times and subjected to SDS–PAGE on a 7.5% Tris-glycine gel, a 4–12% precast gel or a 50 μM phos-tag containing gel. Red asterisks show phosphorylated PINK1. We routinely used HeLa cells and immunoblotting analysis was conducted with an anti-PINK1 antibody unless otherwise specified. (**d**) *In vitro* synthesized PINK1-3HA and the mitochondrial fraction of PINK1-3HA-expressing cells following CCCP treatment were subjected to immunoblotting. (**e**) The cell lysate and immunoprecipitated product of *PINK1*$^{-/-}$ MEFs-expressing WT or the PINK1 KD mutant were subjected to SDS–PAGE on a 7.5% Tris-glycine gel ±50 μM phos-tag. Red asterisks show phosphorylated PINK1. (**f**) The endogenous PINK1 in HeLa cells exists as the phosphorylated form. The black asterisk indicates a cross-reacting band and red asterisks show phosphorylated PINK1. (**g**) Phosphatase treatment caused the high-molecular shift of both exogenous and endogenous PINK1 to disappear. The mitochondrial fraction collected from HeLa cells-expressing PINK1-HA or collected from noninfected HeLa cells was treated with CIAP at the indicated temperature. Exogenous PINK1 was detected with an anti-HA antibody. + and + + mean 10 and 30 U per reaction of CIAP, respectively. (**h**) Cells expressing exogenous PINK1 were treated with CCCP (10 μM, 1 h), valinomycin (10 μM, 1 h) or rotenone (200 μM, 24 h) and subjected to SDS–PAGE on a 7.5% Tris-glycine gel ±50 μM phos-tag.

This abolished the high-molecular-weight shift of not only exogenous PINK1 but also endogenous PINK1 (Fig. 1g). PINK1 phosphorylation was also observed when cells were treated with valinomycin (another type of mitochondrial uncoupler that functions as a K^+ uniporter) or rotenone (a mitochondrial complex I inhibitor), confirming that phosphorylation is not a CCCP-specific event (Fig. 1h, red asterisks). Taken together, these results suggest that PINK1 undergoes autophosphorylation when the $\Delta\Psi$m is decreased.

PINK1 mutations can interfere with autophosphorylation. To determine whether the aforementioned event is physiologically and pathologically significant, we examined the phosphorylation status of PINK1 harboring various pathogenic mutations that cause early-onset familial PD. We studied nine pathogenic missense mutations; that is, PINK1 harboring the C92F, A168P, E240K, H271Q, G309D, L347P, G386A, G409V or E417G mutations. We also used one pathogenic mutant with an amino-acid insertion in which a CAA codon (coding for glutamine) was inserted upstream of nucleotide 1602 (cytosine) and as a result glutamine was inserted within the carboxy-terminal domain at position 534 (referred to here after as 534insQ)[39]. These PINK1 mutants were serially introduced into HeLa cells, treated with CCCP and their phosphorylation status examined. PINK1 with the C92F mutation underwent phosphorylation in a manner equivalent to WT PINK1 (Fig. 2a, lane 3). The band pattern of the G309D mutant was different from WT PINK1 in phos-tag PAGE, that is, slower-migrating bands (especially the upper band) were fainter in the G309D mutant than the WT PINK1 (phos-tag panel of Fig. 2a, lane 7). This result suggests that WT PINK1 is multiply phosphorylated whereas phosphorylation of the G309D mutant appears to be not as extensive. In the other pathogenic mutations, PINK1 phosphorylation was severely compromised (Fig. 2a) even though they localized on depolarized mitochondria (Supplementary Fig. S1). Among the pathogenic mutations, the A168P, E240K, G386A and E417G mutations are expected to perturb the Mg^{2+}/ATP-binding pocket of PINK1[40], again suggesting that phosphorylation of PINK1 is derived from autophosphorylation. We next checked the subcellular localization and autoubiquitylation

Parkinson's disease (PD) is one of the most pervasive neurodegenerative diseases, affecting 1% of the population over the age of 65. PD commonly arises sporadically; however, in some cases the disease is familial and inherited. *PINK1* and *PARKIN* are causal genes for hereditary (that is, autosomal recessive) early-onset PD[1,2]. Studies on their functions can consequently provide important insights into the molecular mechanism of disease pathogenesis.

Although the cause of sporadic PD is likely complex, numerous evidences link mitochondrial dysfunction to its pathogenesis; for example, a moderate deficit in mitochondrial electron transport chain complex activity and mutations/deletions of mitochondrial DNA in PD patients have repeatedly been reported[3,4]. In 2008, Narendra *et al.*[5] reported that Parkin translocates to and degrades depolarized mitochondria following uncoupler treatment. Although this experimental system is an artificial one, it is commonly used as a cellular experimental model for PD that might reflect the intrinsic damage in electron transport chain and the mutations/deletions in mitochondrial DNA that inevitably lead to a decrease in membrane potential ($\Delta\Psi$m).

Newly emergent evidence has shown that PINK1- and Parkin-dependent ubiquitylation has a pivotal role in the quality control of mitochondria, which suggests that dysfunction of either PINK1 or Parkin likely results in the accumulation of low-quality mitochondria, thereby triggering early-onset familial PD. According to the most recently proposed model, selective localization of PINK1 to low-quality mitochondria facilitates the recruitment of cytosolic Parkin to the same mitochondria[6–12]. The ubiquitin ligase activity of Parkin, which is repressed under normal conditions, is re-established on damaged mitochondria[6,13]. Active Parkin then ubiquitylates mitochondrial outer membranous proteins such as Mitofusin, Miro and voltage-dependent anion channel[7,9,10,14–21]. The ubiquitylated proteins and damaged mitochondria are then degraded via the proteasome and autophagy, although the role of PINK1/Parkin in neurons remains controversial[5,19,22–25].

PD-associated PINK1 and Parkin mutations interfere with the ubiquitylation of depolarized mitochondria, suggesting the etiological importance of this process[6–9,12]. During this process, the principal initiation event is the discrimination of damaged mitochondria from their healthy counterparts. A model for this process has recently been described by Youle's group, in which newly synthesized PINK1 is imported to the inner membrane of healthy mitochondria and undergoes mitochondrial protease-dependent cleavage of its amino-terminal domain; the resulting truncated PINK1 is subsequently degraded by the proteasome[26–30]. However, because the $\Delta\Psi$m is required for import, dissipation of $\Delta\Psi$m prevents PINK1 from reaching the inner membrane. As a consequence, PINK1 remains localized to the outer mitochondrial membrane[31–33]. Although this model elegantly explains how the loss of $\Delta\Psi$m causes the accumulation of PINK1 on damaged mitochondria, the molecular mechanisms underlying PINK1 retrieval of Parkin to depolarized mitochondria remain poorly understood.

In this study, we identified two Ser residues (Ser228 and Ser402) in PINK1 that undergo autophosphorylation upon dissipation of mitochondrial $\Delta\Psi$m in cells and determined that these autophosphorylation events are imperative for the efficient retrieval of Parkin to the same mitochondria.

Results

PINK1 regulation by mitochondrial $\Delta\Psi$m. If the essence of PINK1 regulation by mitochondrial $\Delta\Psi$m is only the accumulation of PINK1, increasing the amount of PINK1 should bypass the requirement of $\Delta\Psi$m to recruit Parkin onto mitochondria. When green fluorescent protein (GFP)-Parkin and PINK1 were co-transfected in HeLa cells under the control of a strong cytomegalovirus (CMV)-derived promoter, GFP-Parkin localized on mitochondria regardless of $\Delta\Psi$m as reported previously[7]. However, the Parkin-recruitment activity of over-produced PINK1 was less than the Parkin-recruitment activity of endogenous PINK1 in the presence of the mitochondrial uncoupler carbonyl cyanide *m*-chlorophenylhydrazone (CCCP; Fig. 1a), as immunoblotting confirmed that the amount of exogenous wild-type (WT) PINK1 was much more than that of endogenous PINK1 (Fig. 1b, compare lane 1 with 3). This result indicates that endogenous PINK1 in the presence of the uncoupler more efficiently recruits Parkin to mitochondria than exogenous over-produced PINK1 in the absence of the uncoupler, and suggests that PINK1 is regulated not only quantitatively but also qualitatively in response to a decrease in mitochondrial $\Delta\Psi$m.

We next examined how aside from quantitative regulation PINK1 is regulated by the mitochondrial $\Delta\Psi$m. When HeLa cells harboring exogenous PINK1 were treated with CCCP, we realized that full-length PINK1 resolves as a doublet in immunoblots on conventional handmade 7.5% gels (Fig. 1c). The higher-molecular-weight band is rapidly observed within 30 min of CCCP treatment. This doublet is poorly resolved on commercially available precast gels (Fig. 1c), thus explaining why the doublet was not clear in our previous work[6]. Doublet formation of PINK1 is not derived from processing but rather results from post-translational modification because the molecular size of *in vitro* synthesized PINK1 corresponds to that of the lower PINK1 doublet band (Fig. 1d). To determine whether phosphorylation accounts for this modification, we performed electrophoresis using polyacrylamide gels conjugated with a 1,3-bis(bis(pyridin-2-ylmethyl)amino)propan-2-olato diMn(II) complex (referred to hereafter as Phos-tag). Phos-tag can capture phosphomonoester dianions ($ROPO_3^{2-}$) and thus acrylamide-pendant phos-tag specifically retards the migration of phosphorylated proteins, which are visualized as slower-migrating bands compared with the corresponding nonphosphorylated proteins[34]. When exogenous PINK1 was subjected to polyacrylamide gel electrophoresis (PAGE)-containing phos-tag, a clear mobility shift of full-length PINK1 was observed, suggesting that PINK1 is phosphorylated following CCCP treatment (phos-tag panel of Fig. 1c, shown by red asterisks). PINK1 phosphorylation likely involves multiple sites because two higher-molecular-weight bands are observed. We next examined whether a kinase-dead (KD) mutation (K219A, D362A and D384A) that abolishes PINK1 kinase activity[35] prevents the appearance of this phosphorylated band. To avoid the effects of endogenous PINK1, we used mouse embryonic fibroblasts (MEFs) derived from a *PINK1* knockout (*PINK1*$^{-/-}$) mouse[36] transformed with PINK1-Flag. In those cells, CCCP treatment resulted in a PINK1 doublet on a conventional 7.5% PAGE with the upper band clearly retarded in phos-tag-PAGE (Fig. 1e, asterisks in lane 2). The phosphorylated PINK1 band, however, was completely absent on both 7.5% and phos-tag PAGE in the KD mutant (Fig. 1e, lane 4), suggesting autophosphorylation. Clearer results were obtained following immunoprecipitation with an anti-Flag antibody (Fig. 1e, lanes 5–8).

We next checked whether endogenous PINK1 is also phosphorylated. As reported previously, the endogenous PINK1 signal was barely detectable under steady-state healthy conditions (lane 1 of Fig. 1f), whereas CCCP treatment promoted the emergence of endogenous PINK1 (indicated by the red asterisk in lane 2 of Fig. 1f)[6,7,37,38]. Compared with exogenous non-tagged PINK1, CCCP treatment caused endogenous PINK1 to resolve at a slightly higher-molecular weight (compare lane 2 with 3 of Fig. 1f) and its mobility was consistent with the upper phosphorylated form of exogenous non-tagged PINK1 (compare lane 2 with 4). Phos-tag PAGE confirmed that the endogenous PINK1 that accumulated following CCCP treatment is the phosphorylated form (Fig. 1f, lanes 6–8). To more convincingly demonstrate that PINK1 is phosphorylated, a mitochondrial fraction prepared from CCCP-treated cells was incubated with calf intestinal alkaline phosphatase (CIAP).

nature COMMUNICATIONS

OPEN

ARTICLE

Received 12 Apr 2012 | Accepted 20 Jul 2012 | Published 21 Aug 2012

DOI: 10.1038/ncomms2016

PINK1 autophosphorylation upon membrane potential dissipation is essential for Parkin recruitment to damaged mitochondria

Kei Okatsu[1,2], Toshihiko Oka[3], Masahiro Iguchi[1], Kenji Imamura[1,2], Hidetaka Kosako[4], Naoki Tani[4], Mayumi Kimura[1], Etsu Go[1], Fumika Koyano[1,2], Manabu Funayama[5], Kahori Shiba-Fukushima[5], Shigeto Sato[5], Hideaki Shimizu[6], Yuko Fukunaga[7], Hisaaki Taniguchi[4], Masaaki Komatsu[8], Nobutaka Hattori[5], Katsuyoshi Mihara[7], Keiji Tanaka[1] & Noriyuki Matsuda[1]

Dysfunction of PINK1, a mitochondrial Ser/Thr kinase, causes familial Parkinson's disease (PD). Recent studies have revealed that PINK1 is rapidly degraded in healthy mitochondria but accumulates on the membrane potential ($\Delta\Psi$m)-deficient mitochondria, where it recruits another familial PD gene product, Parkin, to ubiquitylate the damaged mitochondria. Despite extensive study, the mechanism underlying the homeostatic control of PINK1 remains unknown. Here we report that PINK1 is autophosphorylated following a decrease in $\Delta\Psi$m and that most disease-relevant mutations hinder this event. Mass spectrometric and mutational analyses demonstrate that PINK1 autophosphorylation occurs at Ser228 and Ser402, residues that are structurally clustered together. Importantly, Ala mutation of these sites abolishes autophosphorylation of PINK1 and inhibits Parkin recruitment onto depolarized mitochondria, whereas Asp (phosphorylation-mimic) mutation promotes mitochondrial localization of Parkin even though autophosphorylation was still compromised. We propose that autophosphorylation of Ser228 and Ser402 in PINK1 is essential for efficient mitochondrial localization of Parkin.

[1] Laboratory of Protein Metabolism, Tokyo Metropolitan Institute of Medical Science, Setagaya-ku, 156-8506, Japan. [2] Department of Medical Genome Sciences, Graduate School of Frontier Sciences, The University of Tokyo, Kashiwa, Chiba 277-8561, Japan. [3] Department of Life Science, College of Science, Rikkyo University, Toshimaku-ku, Tokyo 171-8501, Japan. [4] Division of Disease Proteomics, Institute for Enzyme Research, The University of Tokushima, 770-8503, Japan. [5] Department of Neurology, Juntendo University School of Medicine, Bunkyo-ku, Tokyo 113-8421, Japan. [6] RIKEN Systems and Structural Biology Center, 1-7-22 Suehiro-cho, Tsurumi-ku, Yokohama 230-0045, Japan. [7] Department of Molecular Biology, Graduate School of Medical Science, Kyushu University, Fukuoka 812-8582, Japan. [8] Protein Metabolism Project, Tokyo Metropolitan Institute of Medical Science, Setagaya-ku, 156-8506, Japan. Correspondence and requests for materials should be addressed to N.M. (email: matsuda-nr@igakuken.or.jp).

22. **Kitada T,** Asakawa S, Hattori N, *et al*. Mutations in the parkin gene cause autosomal recessive juvenile parkinsonism. *Nature* 1998;**392**:605—8.
23. **Hattori N,** Kitada T, Matsumine H, *et al*. Molecular genetic analysis of a novel parkin gene in Japanese families with autosomal recessive juvenile parkinsonism: evidence for variable homozygous deletions in the parkin gene in affected individuals. *Ann Neurol* 1998;**44**:935—41.
24. **Matsumine H,** Saito M, Shimoda-Matsubayashi S, *et al*. Localization of a gene for an autosomal recessive form of juvenile Parkinsonism to chromosome 6q25.2-27. *Am J Hum Genet* 1997;**60**:588—96.
25. **Mori H,** Kondo T, Yokochi M, *et al*. Pathologic and biochemical studies of juvenile parkinsonism linked to chromosome 6q. *Neurology* 1998;**51**:890—2.
26. **Takahashi H,** Ohama E, Suzuki S, *et al*. Familial juvenile parkinsonism: clinical and pathologic study in a family. *Neurology* 1994;**44**:437—41.
27. **Farrer M,** Chan P, Chen R, *et al*. Lewy bodies and parkinsonism in families with parkin mutations. *Ann Neurol* 2001;**50**:293—300.
28. **Hilker R,** Klein C, Ghaemi M, *et al*. Positron emission tomographic analysis of the nigrostriatal dopaminergic system in familial parkinsonism associated with mutations in the parkin gene. *Ann Neurol* 2001;**49**:367—76.
29. **Khan NL,** Brooks DJ, Pavese N, *et al*. Progression of nigrostriatal dysfunction in a parkin kindred: an [18F]dopa PET and clinical study. *Brain* 2002;**125**:2248—56.
30. **Klein C,** Pramstaller PP, Kis B, *et al*. Parkin deletions in a family with adult-onset, tremor-dominant parkinsonism: expanding the phenotype. *Ann Neurol* 2000;**48**:65—71.
31. **Pramstaller PP,** Kis B, Eskelson C, *et al*. Phenotypic variability in a large kindred (Family LA) with deletions in the parkin gene. *Mov Disord* 2002;**17**:424—6.
32. **Lincoln SJ,** Maraganore DM, Lesnick TG, *et al*. Parkin variants in North American Parkinson's disease: cases and controls. *Mov Disord* 2003;**18**:1306—11.
33. **Kay DM,** Moran D, Moses L, *et al*. Heterozygous parkin point mutations are as common in control subjects as in Parkinson's patients. *Ann Neurol* 2007;**61**:47—54.
34. **Shimura H,** Hattori N, Kubo S, *et al*. Familial Parkinson disease gene product, parkin, is a ubiquitin-protein ligase. *Nat Genet* 2000;**25**:302—5.
35. **Matsuda N,** Kitami T, Suzuki T, *et al*. Diverse effects of pathogenic mutations of Parkin that catalyze multiple monoubiquitylation in vitro. *J Biol Chem* 2006;**281**:3204—9.
36. **Shimura H,** Schlossmacher MG, Hattori N, *et al*. Ubiquitination of a new form of alpha-synuclein by parkin from human brain: implications for Parkinson's disease. *Science* 2001;**293**:263—9.
37. **Chung KK,** Zhang Y, Lim KL, *et al*. Parkin ubiquitinates the alpha-synuclein-interacting protein, synphilin-1: implications for Lewy-body formation in Parkinson disease. *Nat Med* 2001;**7**:1144—50.
38. **Weihofen A,** Thomas KJ, Ostaszewski BL, *et al*. Pink1 forms a multiprotein complex with Miro and Milton, linking Pink1 function to mitochondrial trafficking (dagger). *Biochemistry* 2009;**48**:2045—52.
39. **Narendra D,** Tanaka A, Suen DF, *et al*. Parkin is recruited selectively to impaired mitochondria and promotes their autophagy. *J Cell Biol* 2008;**183**:795—803.
40. **Narendra D,** Kane LA, Hauser DN, *et al*. p62/SQSTM1 is required for Parkin-induced mitochondrial clustering but not mitophagy; VDAC1 is dispensable for both. *Autophagy* 2010;**6**:1090—106.
41. **Matsuda N,** Sato S, Shiba K, *et al*. PINK1 stabilized by mitochondrial depolarization recruits Parkin to damaged mitochondria and activates latent Parkin for mitophagy. *J Cell Biol* 2010;**189**:211—21.
42. **Park J,** Lee G, Chung J. The PINK1—Parkin pathway is involved in the regulation of mitochondrial remodeling process. *Biochem Biophys Res Commun* 2009;**378**:518—23.
43. **Valente EM,** Bentivoglio AR, Dixon PH, *et al*. Localization of a novel locus for autosomal recessive early-onset parkinsonism, PARK6, on human chromosome 1p35-p36. *Am J Hum Genet* 2001;**68**:895—900.
44. **Valente EM,** Abou-Sleiman PM, Caputo V, *et al*. Hereditary early-onset Parkinson's disease caused by mutations in PINK1. *Science* 2004;**304**:1158—60.
45. **Marongiu R,** Brancati F, Antonini A, *et al*. Whole gene deletion and splicing mutations expand the PINK1 genotypic spectrum. *Hum Mutat* 2007;**28**:98.
46. **Hatano Y,** Li Y, Sato K, *et al*. Novel PINK1 mutations in early-onset parkinsonism. *Ann Neurol* 2004;**56**:424—7.
47. **Samaranch L,** Lorenzo-Betancor O, Arbelo JM, *et al*. PINK1-linked parkinsonism is associated with Lewy body pathology. *Brain* 2010;**133**:1128—42.
48. **Kawajiri S,** Saiki S, Sato S, *et al*. Genetic mutations and functions of PINK1. *Trends Pharmacol Sci* 2011;**32**:573—80.
49. **Beilina A,** Van Der Brug M, Ahmad R, *et al*. Mutations in PTEN-induced putative kinase 1 associated with recessive parkinsonism have differential effects on protein stability. *Proc Natl Acad Sci U S A* 2005;**102**:5703—8.
50. **Pridgeon JW,** Olzmann JA, Chin LS, *et al*. PINK1 protects against oxidative stress by phosphorylating mitochondrial chaperone TRAP1. *PLoS Biol* 2007;**5**:e172.
51. **Silvestri L,** Caputo V, Bellacchio E, *et al*. Mitochondrial import and enzymatic activity of PINK1 mutants associated to recessive parkinsonism. *Hum Mol Genet* 2005;**14**:3477—92.
52. **Sim CH,** Lio DS, Mok SS, *et al*. C-terminal truncation and Parkinson's disease-associated mutations down-regulate the protein serine/threonine kinase activity of PTEN-induced kinase-1. *Hum Mol Genet* 2006;**15**:3251—62.
53. **Murata H,** Sakaguchi M, Jin Y, *et al*. A new cytosolic pathway from a Parkinson disease-associated kinase, BRPK/PINK1: activation of AKT via mTORC2. *J Biol Chem* 2011;**286**:7182—9.
54. **Plun-Favreau H,** Klupsch K, Moisoi N, *et al*. The mitochondrial protease HtrA2 is regulated by Parkinson's disease-associated kinase PINK1. *Nat Cell Biol* 2007;**9**:1243—52.
55. **Strauss KM,** Martins LM, Plun-Favreau H, *et al*. Loss of function mutations in the gene encoding Omi/HtrA2 in Parkinson's disease. *Hum Mol Genet* 2005;**14**:2099—111.
56. **Wang X,** Schwarz TL. The mechanism of Ca2+ -dependent regulation of kinesin-mediated mitochondrial motility. *Cell* 2009;**136**:163—74.
57. **Liu W,** Vives-Bauza C, Acin-Perez R, *et al*. PINK1 defect causes mitochondrial dysfunction, proteasomal deficit and alpha-synuclein aggregation in cell culture models of Parkinson's disease. *PLoS One* 2009;**4**:e4597.
58. **Amo T,** Sato S, Saiki S, *et al*. Mitochondrial membrane potential decrease caused by loss of PINK1 is not due to proton leak, but to respiratory chain defects. *Neurobiol Dis* 2011;**41**:111—8.
59. **Deng H,** Dodson MW, Huang H, *et al*. The Parkinson's disease genes pink1 and parkin promote mitochondrial fission and/or inhibit fusion in Drosophila. *Proc Natl Acad Sci U S A* 2008;**105**:14503—8.
60. **Poole AC,** Thomas RE, Andrews LA, *et al*. The PINK1/Parkin pathway regulates mitochondrial morphology. *Proc Natl Acad Sci U S A* 2008;**105**:1638—43.
61. **Haque ME,** Thomas KJ, D'Souza C, *et al*. Cytoplasmic Pink1 activity protects neurons from dopaminergic neurotoxin MPTP. *Proc Natl Acad Sci U S A* 2008;**105**:1716—21.
62. **Clark IE,** Dodson MW, Jiang C, *et al*. Drosophila pink1 is required for mitochondrial function and interacts genetically with parkin. *Nature* 2006;**441**:1162—6.
63. **Park J,** Lee SB, Lee S, *et al*. Mitochondrial dysfunction in Drosophila PINK1 mutants is complemented by parkin. *Nature* 2006;**441**:1157—61.
64. **Yang Y,** Gehrke S, Imai Y, *et al*. Mitochondrial pathology and muscle and dopaminergic neuron degeneration caused by inactivation of Drosophila Pink1 is rescued by Parkin. *Proc Natl Acad Sci U S A* 2006;**103**:10793—8.
65. **Kawajiri S,** Saiki S, Sato S, *et al*. PINK1 is recruited to mitochondria with parkin and associates with LC3 in mitophagy. *FEBS Lett* 2010;**584**:1073—9.
66. **Youle RJ,** Narendra DP. Mechanisms of mitophagy. *Nat Rev Mol Cell Biol* 2011;**12**:9—14.
67. **Abou-Sleiman PM,** Healy DG, Quinn N, *et al*. The role of pathogenic DJ-1 mutations in Parkinson's disease. *Ann Neurol* 2003;**54**:283—6.
68. **Bandopadhyay R,** Kingsbury AE, Cookson MR, *et al*. The expression of DJ-1 (PARK7) in normal human CNS and idiopathic Parkinson's disease. *Brain* 2004;**127**:420—30.
69. **Neumann M,** Muller V, Gorner K, *et al*. Pathological properties of the Parkinson's disease-associated protein DJ-1 in alpha-synucleinopathies and tauopathies: relevance for multiple system atrophy and Pick's disease. *Acta Neuropathol* 2004;**107**:489—96.
70. **Olzmann JA,** Bordelon JR, Muly EC, *et al*. Selective enrichment of DJ-1 protein in primate striatal neuronal processes: implications for Parkinson's disease. *J Comp Neurol* 2007;**500**:585—99.
71. **Usami Y,** Hatano T, Imai S, *et al*. DJ-1 associates with synaptic membranes. *Neurobiol Dis* 2011;**43**:651—62.
72. **Miller DW,** Ahmad R, Hague S, *et al*. L166P mutant DJ-1, causative for recessive Parkinson's disease, is degraded through the ubiquitin-proteasome system. *J Biol Chem* 2003;**278**:36588—95.
73. **Goldberg MS,** Pisani A, Haburcak M, *et al*. Nigrostriatal dopaminergic deficits and hypokinesia caused by inactivation of the familial parkinsonism-linked gene DJ-1. *Neuron* 2005;**45**:489—96.
74. **Wang Z,** Liu J, Chen S, *et al*. DJ-1 modulates the expression of Cu/Zn-superoxide dismutase-1 through the Erk1/2-Elk1 pathway in neuroprotection. *Ann Neurol* 2011;**70**:591—9.
75. **Lev N,** Roncevic D, Ickowicz D, *et al*. Role of DJ-1 in Parkinson's disease. *J Mol Neurosci* 2006;**29**:215—25.
76. **Fu K,** Ren H, Wang Y, *et al*. DJ-1 inhibits TRAIL-induced apoptosis by blocking pro-caspase-8 recruitment to FADD. *Oncogene*. Published Online First: 25 July 2011. doi:10.1038/onc.2011.315.
77. **Xiong H,** Wang D, Chen L, *et al*. Parkin, PINK1, and DJ-1 form a ubiquitin E3 ligase complex promoting unfolded protein degradation. *J Clin Invest* 2009;**119**:650—60.
78. **Paisan-Ruiz C,** Jain S, Evans EW, *et al*. Cloning of the gene containing mutations that cause PARK8-linked Parkinson's disease. *Neuron* 2004;**44**:595—600.
79. **Zimprich A,** Biskup S, Leitner P, *et al*. Mutations in LRRK2 cause autosomal-dominant parkinsonism with pleomorphic pathology. *Neuron* 2004;**44**:601—7.
80. **Berwick DC,** Harvey K. LRRK2 signaling pathways: the key to unlocking neurodegeneration? *Trends Cell Biol* 2011;**21**:257—65.
81. **Cookson MR.** The role of leucine-rich repeat kinase 2 (LRRK2) in Parkinson's disease. *Nat Rev Neurosci* 2010;**11**:791—7.
82. **Gilks WP,** Abou-Sleiman PM, Gandhi S, *et al*. A common LRRK2 mutation in idiopathic Parkinson's disease. *Lancet* 2005;**365**:415—16.
83. **Wszolek ZK,** Pfeiffer RF, Tsuboi Y, *et al*. Autosomal dominant parkinsonism associated with variable synuclein and tau pathology. *Neurology* 2004;**62**:1619—22.
84. **Ross OA,** Toft M, Whittle AJ, *et al*. Lrrk2 and Lewy body disease. *Ann Neurol* 2006;**59**:388—93.
85. **Dachsel JC,** Ross OA, Mata IF, *et al*. Lrrk2 G2019S substitution in frontotemporal lobar degeneration with ubiquitin-immunoreactive neuronal inclusions. *Acta Neuropathol* 2007;**113**:601—6.

86. **Galter D,** Westerlund M, Carmine A, *et al*. LRRK2 expression linked to dopamine-innervated areas. *Ann Neurol* 2006;**59**:714—19.
87. **Hatano T,** Kubo S, Imai S, *et al*. Leucine-rich repeat kinase 2 associates with lipid rafts. *Hum Mol Genet* 2007;**16**:678—90.
88. **Biskup S,** Moore DJ, Celsi F, *et al*. Localization of LRRK2 to membranous and vesicular structures in mammalian brain. *Ann Neurol* 2006;**60**:557—69.
89. **Smith WW,** Pei Z, Jiang H, *et al*. Leucine-rich repeat kinase 2 (LRRK2) interacts with parkin, and mutant LRRK2 induces neuronal degeneration. *Proc Natl Acad Sci U S A* 2005;**102**:18676—81.
90. **Ng CH,** Mok SZ, Koh C, *et al*. Parkin protects against LRRK2 G2019S mutant-induced dopaminergic neurodegeneration in Drosophila. *J Neurosci* 2009;**29**:11257—62.
91. **Venderova K,** Kabbach G, Abdel-Messih E, *et al*. Leucine-rich repeat kinase 2 interacts with parkin, DJ-1 and PINK-1 in a Drosophila melanogaster model of Parkinson's disease. *Hum Mol Genet* 2009;**18**:4390—404.
92. **Chan D,** Citro A, Cordy JM, *et al*. Rac1 protein rescues neurite retraction caused by G2019S leucine-rich repeat kinase 2 (LRRK2). *J Biol Chem* 2011;**286**:16140—9.
93. **Angeles DC,** Gan BH, Onstead L, *et al*. Mutations in LRRK2 increase phosphorylation of peroxiredoxin 3 exacerbating oxidative stress-induced neuronal death. *Hum Mutat* 2011;**32**:1390—7.
94. **Dusonchet J,** Kochubey O, Stafa K, *et al*. A rat model of progressive nigral neurodegeneration induced by the Parkinson's disease-associated G2019S mutation in LRRK2. *J Neurosci* 2011;**31**:907—12.
95. **Li X,** Wang QJ, Pan N, *et al*. Phosphorylation-dependent 14-3-3 binding to LRRK2 is impaired by common mutations of familial Parkinson's disease. *PLoS One* 2011;**6**: e17153.
96. **Najim al-Din AS,** Wriekat A, Mubaidin A, *et al*. Pallido-pyramidal degeneration, supranuclear upgaze paresis and dementia: Kufor-Rakeb syndrome. *Acta Neurol Scand* 1994;**89**:347—52.
97. **Ramirez A,** Heimbach A, Grundemann J, *et al*. Hereditary parkinsonism with dementia is caused by mutations in ATP13A2, encoding a lysosomal type 5 P-type ATPase. *Nat Genet* 2006;**38**:1184—91.
98. **Gitler AD,** Chesi A, Geddie ML, *et al*. Alpha-synuclein is part of a diverse and highly conserved interaction network that includes PARK9 and manganese toxicity. *Nat Genet* 2009;**41**:308—15.
99. **Ugolino J,** Fang S, Kubisch C, *et al*. Mutant Atp13a2 proteins involved in parkinsonism are degraded by ER-associated degradation and sensitize cells to ER-stress induced cell death. *Hum Mol Genet* 2011;**20**:3565—77.
100. **Tan J,** Zhang T, Jiang L, *et al*. Regulation of intracellular manganese hemeostasis by kufor-rakeb syndrome associated ATP13A2. *J Biol Chem* 2011;**286**:29654—62.
101. **Kawamoto Y,** Kobayashi Y, Suzuki Y, *et al*. Accumulation of HtrA2/Omi in neuronal and glial inclusions in brains with alpha-synucleinopathies. *J Neuropathol Exp Neurol* 2008;**67**:984—93.
102. **Kruger R,** Sharma M, Riess O, *et al*. A large-scale genetic association study to evaluate the contribution of Omi/HtrA2 (PARK13) to Parkinson's disease. *Neurobiol Aging* 2011;**32**:548 e9—18.
103. **Suzuki Y,** Takahashi-Niki K, Akagi T, *et al*. Mitochondrial protease Omi/HtrA2 enhances caspase activation through multiple pathways. *Cell Death Differ* 2004;**11**:208—16.
104. **Martins LM.** The serine protease Omi/HtrA2: a second mammalian protein with a reaper-like function. *Cell Death Differ* 2002;**9**:699—701.
105. **Martins LM,** Morrison A, Klupsch K, *et al*. Neuroprotective role of the reaper-related serine protease HtrA2/Omi revealed by targeted deletion in mice. *Mol Cell Biol* 2004;**24**:9848—62.
106. **Li B,** Hu Q, Wang H, *et al*. Omi/HtrA2 is a positive regulator of autophagy that facilitates the degradation of mutant proteins involved in neurodegenerative diseases. *Cell Death Differ* 2010;**17**:1773—84.
107. **Morgan NV,** Westaway SK, Morton JE, *et al*. PLA2G6, encoding a phospholipase A2, is mutated in neurodegenerative disorders with high brain iron. *Nat Genet* 2006;**38**:752—4.
108. **Paisan-Ruiz C,** Bhatia KP, Li A, *et al*. Characterization of PLA2G6 as a locus for dystonia-parkinsonism. *Ann Neurol* 2009;**65**:19—23.
109. **Yoshino H,** Tomiyama H, Tachibana N, *et al*. Phenotypic spectrum of patients with PLA2G6 mutation and PARK14-linked parkinsonism. *Neurology* 2010;**75**:1356—61.
110. **Jenkins CM,** Wolf MJ, Mancuso DJ, *et al*. Identification of the calmodulin-binding domain of recombinant calcium-independent phospholipase A2beta. Implications for structure and function. *J Biol Chem* 2001;**276**:7129—35.
111. **Wang Z,** Ramanadham S, Ma ZA, *et al*. Group VIA phospholipase A2 forms a signaling complex with the calcium/calmodulin-dependent protein kinase IIbeta expressed in pancreatic islet beta-cells. *J Biol Chem* 2005;**280**:6840—9.
112. **Shojaee S,** Sina F, Banihosseini SS, *et al*. Genome-wide linkage analysis of a Parkinsonian-pyramidal syndrome pedigree by 500 K SNP arrays. *Am J Hum Genet* 2008;**82**:1375—84.
113. **Di Fonzo A,** Dekker MC, Montagna P, *et al*. FBXO7 mutations cause autosomal recessive, early-onset parkinsonian-pyramidal syndrome. *Neurology* 2009;**72**:240—5.
114. **Pankratz N,** Wilk JB, Latourelle JC, *et al*. Genomewide association study for susceptibility genes contributing to familial Parkinson disease. *Hum Genet* 2009;**124**:593—605.
115. **Edwards TL,** Scott WK, Almonte C, *et al*. Genome-wide association study confirms SNPs in SNCA and the MAPT region as common risk factors for Parkinson disease. *Ann Hum Genet* 2010;**74**:97—109.
116. **Hamza TH,** Zabetian CP, Tenesa A, *et al*. Common genetic variation in the HLA region is associated with late-onset sporadic Parkinson's disease. *Nat Genet* 2010;**42**:781—5.
117. **Spencer CC,** Plagnol V, Strange A, *et al*. Dissection of the genetics of Parkinson's disease identifies an additional association 5' of SNCA and multiple associated haplotypes at 17q21. *Hum Mol Genet* 2010;**20**:345—53.
118. **Liu X,** Cheng R, Verbitsky M, *et al*. Genome-wide association study identifies candidate genes for Parkinson's disease in an Ashkenazi Jewish population. *BMC Med Genet* 2011;**12**:104.
119. **Do CB,** Tung JY, Dorfman E, *et al*. Web-based genome-wide association study identifies two novel Loci and a substantial genetic component for Parkinson's disease. *PLoS Genet* 2011;**7**:e1002141.
120. **Hruska KS,** Goker-Alpan O, Sidransky E. Gaucher disease and the synucleinopathies. *J Biomed Biotechnol* 2006;**2006**:78549.
121. **Sidransky E,** Nalls MA, Aasly JO, *et al*. Multicenter analysis of glucocerebrosidase mutations in Parkinson's disease. *N Engl J Med* 2009;**361**:1651—61.
122. **Aharon-Peretz J,** Rosenbaum H, Gershoni-Baruch R. Mutations in the glucocerebrosidase gene and Parkinson's disease in Ashkenazi Jews. *N Engl J Med* 2004;**351**:1972—7.
123. **Mata IF,** Samii A, Schneer SH, *et al*. Glucocerebrosidase gene mutations: a risk factor for Lewy body disorders. *Arch Neurol* 2008;**65**:379—82.
124. **De Marco EV,** Annesi G, Tarantino P, *et al*. Glucocerebrosidase gene mutations are associated with Parkinson's disease in southern Italy. *Mov Disord* 2008;**23**:460—3.
125. **Morris HR,** Lees AJ, Wood NW. Neurofibrillary tangle parkinsonian disorders—tau pathology and tau genetics. *Mov Disord* 1999;**14**:731—6.
126. **Galpern WR,** Lang AE. Interface between tauopathies and synucleinopathies: a tale of two proteins. *Ann Neurol* 2006;**59**:449—58.
127. **Tayebi N,** Walker J, Stubblefield B, *et al*. Gaucher disease with parkinsonian manifestations: does glucocerebrosidase deficiency contribute to a vulnerability to parkinsonism? *Mol Genet Metab* 2003;**79**:104—9.
128. **Goker-Alpan O,** Stubblefield BK, Giasson BI, *et al*. Glucocerebrosidase is present in alpha-synuclein inclusions in Lewy body disorders. *Acta Neuropathol* 2010;**120**:641—9.
129. **Cullen V,** Sardi SP, Ng J, *et al*. Acid beta-glucosidase mutants linked to Gaucher disease, Parkinson disease, and Lewy body dementia alter alpha-synuclein processing. *Ann Neurol* 2011;**69**:940—53.
130. **Yap TL,** Gruschus JM, Velayati A, *et al*. Alpha-synuclein interacts with glucocerebrosidase providing a molecular link between Parkinson and Gaucher diseases. *J Biol Chem* 2011;**286**:28080—8.
131. **Hardy J.** No definitive evidence for a role for the environment in the etiology of Parkinson's disease. *Mov Disord* 2006;**21**:1790—1.
132. **Deng X,** Dzamko N, Prescott A, *et al*. Characterization of a selective inhibitor of the Parkinson's disease kinase LRRK2. *Nat Chem Biol* 2011;**7**:203—5.

Molecular pathogenesis of Parkinson's disease: update

Shinji Saiki, Shigeto Sato and Nobutaka Hattori

J Neurol Neurosurg Psychiatry 2012 83: 430-436 originally published online December 3, 2011
doi: 10.1136/jnnp-2011-301205

BRIEF REPORT

Pseudo-heterozygous Rearrangement Mutation of *parkin*

Manabu Funayama, PhD,[1,2*] Hiroyo Yoshino, PhD,[1] Yuanzhe Li, MD, PhD,[1] Hiromichi Kusaka, DB,[2] Hiroyuki Tomiyama, MD, PhD,[2,3] and Nobutaka Hattori, MD, PhD[1,2,3*]

[1]*Research Institute for Diseases of Old Age, Graduate School of Medicine, Juntendo University, Tokyo, Japan;* [2]*Department of Neurology, Juntendo University School of Medicine, Tokyo, Japan;* [3]*Department of Neuroscience for Neurodegenerative Disorders, Juntendo University School of Medicine, Tokyo, Japan*

ABSTRACT

Background: Mutations in *parkin* are the most frequent cause of autosomal recessive parkinsonism. Quantitative PCR is used to detect *parkin* rearrangements. However, the method has an inherent problem—deletion and duplication in the same allelic exon could be determined as normal. To present this misidentification, we report a family with compound heterozygous rearrangements in *parkin*. **Methods:** A patient with early-onset parkinsonism and the parents were investigated by quantitative PCR, haplotype analysis, reverse-transcription PCR, and direct sequencing. **Results:** A single heterozygous duplication (duplication of exons 6–7) was identified in the patient by quantitative PCR. Detailed analysis of the family revealed the patient carried compound heterozygous of combined deletion (deletion of exons 3–5) and duplication (duplication of exons 3–7). **Conclusions:** For correct determination of rearrangement mutation, mutation analysis of the patient as well as other family members and/or break-point analysis of genomic DNA and at the transcript level should be conducted.

Key Words: Parkinson's disease; rearrangement; parkin; compound heterozygote; gene dosage

Parkinson's disease (PD) is the most common progressive neurological movement disorder involving loss of neurons in the substantia nigra. Although most patients have sporadic PD, 5%–10% of patients have a positive family history of PD. Mutations in *parkin* (MIM 602544; *PARK2*) are the most common cause of autosomal recessive early-onset parkinsonism.[1,2] So far, various mutations of *parkin* have been identified including rearrangements (deletions and multiplications) and point mutations.[3–5] In addition, there is controversy about whether a single heterozygous mutation of *parkin* also associates with familial as well as sporadic PD.[6,7] Thus, screening for *parkin* mutations is important to elucidate the pathogenesis of not only *parkin*-linked parkinsonism but also of sporadic PD.

In general, homozygous exonic deletion and point mutations are screened by polymerase chain reaction (PCR) and direct sequencing.[1] Multiplication and single heterozygous exonic deletions are analyzed by quantitative PCR (qPCR).[8] However, there is a limitation in the method of qPCR because exonic rearrangement can be misidentified. For example, compound heterozygous mutations for deletion and duplication in the same allelic exons can be determined as normal.

In the present study, to demonstrate the problem of screening for exonic rearrangement, we applied detailed genetic analysis to investigate *parkin* mutations in a Japanese family with early-onset parkinsonism.

Subjects and Methods

Subjects

This study was approved by the ethics committee of Juntendo University School of Medicine. Each subject provided informed consent. One patient with early-onset parkinsonism and her parents were investigated for *parkin* mutations. Array comparative genomic hybridization analysis confirmed the break point of *PARK2*, as described previously.[9] The index patient was a 21-year-old Japanese woman. She initially showed akinesia with gait disturbance in the right lower limb at age 15. Two years later, the patient developed resting tremor in the upper limb and right

Additional Supporting Information may be found in the online version of this article.

***Correspondence to:** Drs. Manabu Funayama or Nobutaka Hattori, Research Institute for Diseases of Old Age, Graduate School of Medicine, Juntendo University, 2-1-1 Hongo, Bunkyo-ku, Tokyo 113-8421, Japan; funayama@juntendo.ac.jp

Funding agencies: This work was supported by the Strategic Research Foundation Grant-in-Aid Project for Private Universities, Grants-in-Aid for Scientific Research (to N.H., 80218510, and to H.T., 21591098), Grant-in-Aid for Young Scientists (to M.F., 22790829, and to Y.L., 23791003), Grant-in-Aid for Scientific Research on Innovative Areas (to M.F. 23129506) from the Japanese Ministry of Education, Culture, Sports, Science and Technology, and Project Research Grants-in-Aid (to M.F., 1041 and 2334) from Juntendo University School of Medicine.

Relevant conflicts of interest/financial disclosures: Nothing to report. Full financial disclosures and author roles may be found in the online version of this article.

Received: 4 July 2011; **Revised:** 11 November 2011; **Accepted:** 12 December 2011

Published online in Wiley Online Library (wileyonlinelibrary.com).
DOI: 10.1002/mds.24906

lower limb (Hoehn and Yahr stage I). She had a good response to levodopa treatment but developed levodopa-induced dyskinesias during treatment. The parents were nonconsanguineous and free of PD or any other neurodegenerative disease.

Genetic Analysis of *parkin*

Genomic DNA was isolated from peripheral blood using a QIAamp blood Maxi Kit (Qiagen, Valencia, CA). All exons of *parkin* were amplified by PCR. PCR amplicons were separated and visualized by 2% agarose gel electrophoresis. After purification of PCR amplicons using ExoSAP IT (GE Healthcare, Salt Lake City, UT), direct sequencing was carried out by a Big Dye Terminator v1.1 Cycle Sequencing Kit (Applied Biosystems, Foster City, CA) and a 3130 Genetic Analyzer (Applied Biosystems, Foster City, CA). The gene dosage of *parkin* was analyzed by qPCR using TaqMan Fast Universal Master Mix (Applied Biosystems, Foster City, CA) and a 7500 Fast Real-Time PCR system (Applied Biosystems, Foster City, CA).

Semiquantitative haplotype analysis was performed by PCR using fluorescent-labeled primers and 3130 Genetic Analyzer (Applied Biosystems, Foster City, CA). We genotyped 12 microsatellites on the *PARK2* locus including D6S1723, D6S1277, D6S1599, D6S980, D6S955, D6S305, D6S411, AFMa155td9, AFMb281wf1, D6S1579, D6S1035, and D6S2436. The sequences of the primers and the conditions of PCR have been described previously.[1,8] Total RNA was isolated from peripheral blood using a PAXgene Blood RNA Kit (Qiagen, Valencia, CA). Total RNA (500 ng) was used to synthesize cDNA using a TaKaRa RNA PCR Kit (AMV) version 3.0 (Takara Bio, Shiga, Japan) and random 9-mer primer (Takara Bio, Shiga, Japan). The cDNA was amplified by PCR using KOD-FX (TOYOBO, Osaka, Japan), and the following primers: 5′-GTTCCGGCTGACCAGTTGC-3′ and 5′-CCGGTTGTACTGCTCTTCTCCC3′, for detection of deletion; 5′-CCAGTGACCATGATAGTGTT-3′ and 5′-TGAAGGTAGACACTGGGTAT-3′, for detection of multiplication.[10] Reverse-transcriptase PCR (RT-PCR) products were separated and visualized by 2% agarose gel electrophoresis. Subsequently, each of the bands was cut out and eluted using a QIAquick Gel Extraction Kit (Qiagen, Valencia, CA). Purified RT-PCR products were sequenced using a Big Dye Terminator v1.1 Cycle Sequencing Kit (Applied Biosystems, Foster City, CA).

Results

None of the point mutations of *parkin* or homozygous exonic deletions were detected in any of the 3 family members. Heterozygous duplications of exons 6 and 7 (EX6–7 dup) of *parkin* were detected in the patient with parkinsonism by gene dosage analysis using qPCR (Fig. 1). However, the parents did not have the same mutation as the patient. Instead, heterozygous duplications from exons 3–7 (EX3–7 dup) were detected in the father, and heterozygous deletions from exons 3–5 (EX3–5 del) were detected in the mother (Fig. 1).

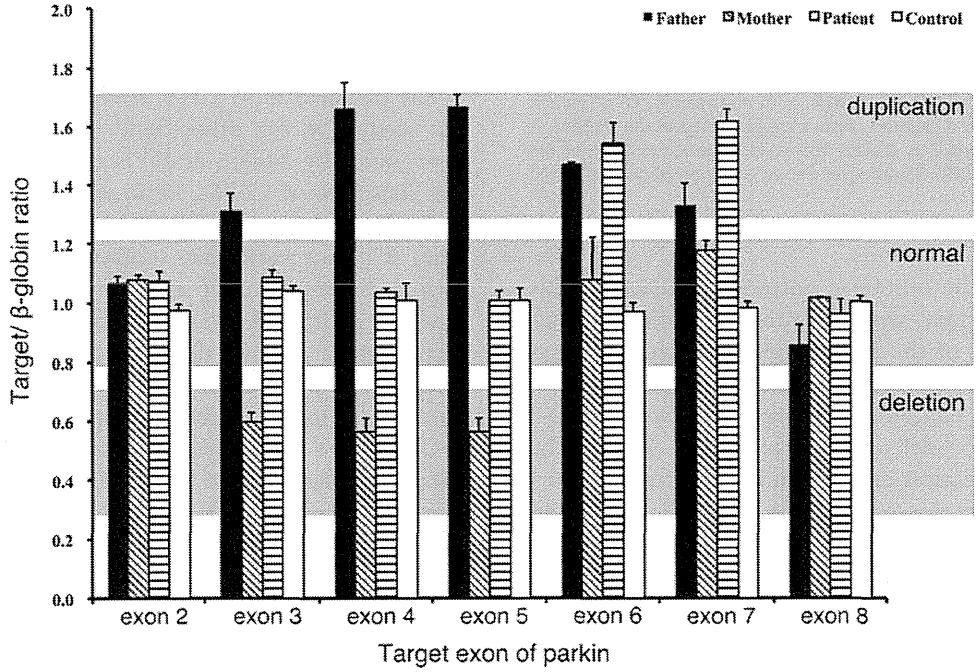

FIG. 1. Gene-dosage analysis of *parkin* using qPCR. Gene dosage of *parkin* was normalized to the dosage of β-*globin*. Values between 0.3 and 0.7 represent heterozygous deletion, between 0.8 and 1.2 are normal, and between 1.3 and 1.7 represent heterozygous duplication. Data are means ± SEMs.

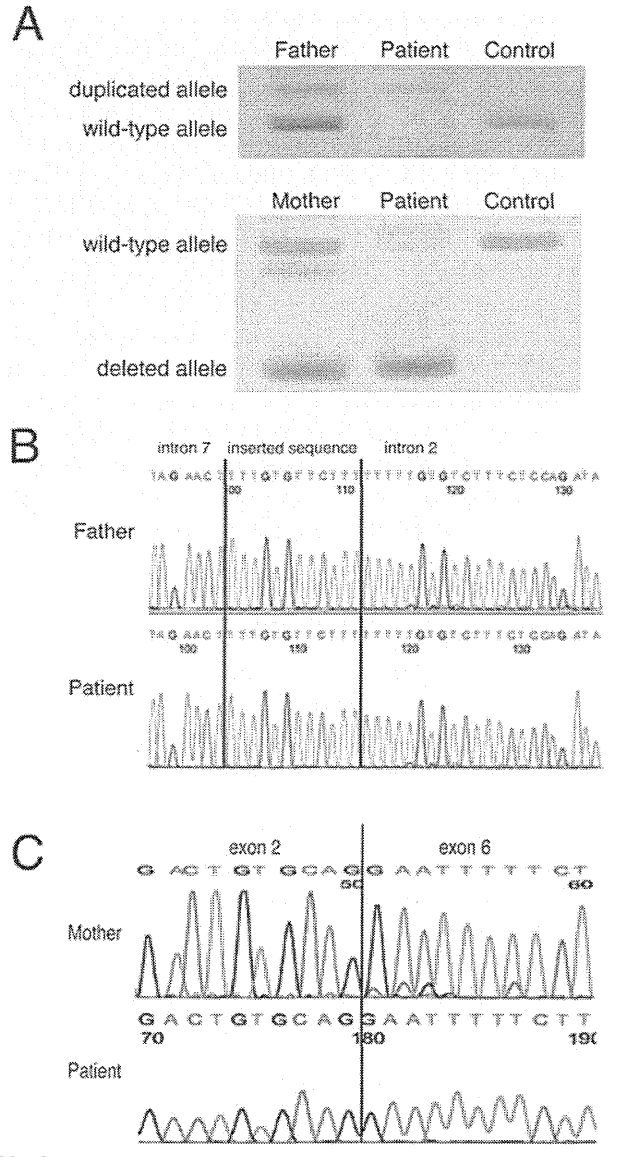

FIG. 2. RT-PCR analysis (**A**) and break-point analysis (**B, C**) of *parkin*. A duplicated allele and a deleted allele were detected in the patient. A break point from introns 7 to 2 was observed in genomic DNA of the patient and the father (**B**). Skipping of exons 3–5 was observed in the *parkin* transcript (**C**).

To determine the mutation pattern of *parkin* in this family, we performed semiquantitative haplotype analysis. Comparison of the peak height of each allele and genotyping results showed a pattern compatible with the patient being compound heterozygous with EX3–7 dup and EX3–5 del (Supporting Fig. 1A,B). To confirm this prediction of the mutation pattern of *parkin* in our patient, we carried out RT-PCR and direct sequencing. The results showed that 2 of the abnormal alleles (EX 3–7dup and EX3–5 del) were inherited from the parents (Fig. 2A–C). Furthermore, the parents harbored a single heterozygous exonic rearrangement of *parkin*. We detected a sequence of the duplicated break point in the patient and the father, and exon skipping of *parkin* was observed at the transcript level in the patient and the mother (Fig. 2A–C). Because recurrent tandem duplication of introns 2–7 of *parkin* have been reported,[9] only 1 break point was observed in the patient and the father (Fig. 2B).

Discussion

Mutations of *parkin* are the most frequent cause of autosomal recessive early-onset parkinsonism, and thus unaffected carriers with single heterozygous *parkin* mutation are thought to exist. In this study, we demonstrated the incorrect determination of *parkin* rearrangement mutation using qPCR assay based on the combination of duplication and deletion in the same allelic exons. This erroneous decision is difficult to avoid by examining gene dosage in only patients with parkinsonism.

Recently, single heterozygous mutations of genes such as *parkin* and *PINK1* associated with autosomal recessive familial parkinsonism were considered risk and modifying factors for sporadic PD as well as familial PD.[6,7,11–13] If a single heterozygous rearrangement in contiguous exons is found by qPCR, it cannot be determined if this rearrangement exists on the same allele. *Parkin* exists in a common fragile site, and exonic rearrangements of *parkin* are frequently reported in patients with parkinsonism from various racial and ethnic groups.[1–5,9] Therefore, it is important to be precise when determining the mutation pattern.

Various methods are currently employed for detection of copy-number variations (CNVs), such as qPCR, multiplex ligation-dependent probe amplification (MLPA), and microarray-based CNV assay.[14] qPCR and MLPA are convenient and rapid methods that use small aliquots of genomic DNA to analyze CNV-mapped limited loci. However, these methods could produce false CNV results, as seen in the present study. On the other hand, the high-density microarray used by Mitsui et al[9] is suitable for determining the structure of CNVs, although it is not designed for routine screening of CNVs. Reflecting on such a situation, it is our view that subjects with a single heterozygous rearrangement mutation of *parkin* should at least be examined by RT-PCR analysis. Although the examination cannot detect the mutation with 100% sensitivity, the observation of transcript formation could be helpful in determining the mutation pattern.

CNVs are associated not only with the heredity form of the disease but also with the sporadic form.[15,16] So far, PD associated with rearrangements of *SNCA*, *PINK1*, and *parkin* have been described.[1,17,18] Interestingly, the severity of PD is influenced by the copy number of *SNCA*.[19] CNVs of certain unknown genes that play a pathogenic role in PD will likely be reported in the future. The copy number of these genes will possibly be important for the prediction of progression of PD. Thus, there is a

need to evaluate CNVs, taking into consideration the copy number of genes.

In conclusion, for correct determination of rearrangement mutation, mutation analysis not only in the patient but also in other family members and/or break-point analysis of genomic DNA and at the transcript level should be conducted. ■

Acknowledgments: We thank all the participants in this study. We also thank Dr. Jun Mitsui for technical advice on break-point analysis, and Ms. Yoko Imamichi for technical assistance.

References

1. Kitada T, Asakawa S, Hattori N, et al. Mutations in the parkin gene cause autosomal recessive juvenile parkinsonism. Nature. 1998;392:605–608.
2. Lücking CB, Dürr A, Bonifati V, et al. Association between early-onset Parkinson's disease and mutations in the parkin gene. N Engl J Med. 2000;342:1560–1567.
3. Nichols WC, Pankratz N, Uniacke SK, et al. Linkage stratification and mutation analysis at the parkin locus identifies mutation positive Parkinson's disease families. J Med Genet. 2002;39:489–492.
4. Lohmann E, Periquet M, Bonifati V, et al. How much phenotypic variation can be attributed to parkin genotype? Ann Neurol. 2003; 54:176–185.
5. Nuytemans K, Theuns J, Cruts M, Van Broeckhoven C. Genetic etiology of Parkinson disease associated with mutations in the SNCA, PARK2, PINK1, PARK7, and LRRK2 genes: a mutation update. Hum Mutat. 2010;7:763–780.
6. Oliveira SA, Scott WK, Martin ER, et al. Parkin mutations and susceptibility alleles in late-onset Parkinson's disease. Ann Neurol. 2003;53:624–629.
7. Kay DM, Stevens CF, Hamza TH, et al. A comprehensive analysis of deletions, multiplications, and copy number variations in PARK2. Neurology. 2010;75:1189–1194.
8. Kobayashi T, Matsumine H, Zhang J, Imamichi Y, Mizuno Y, Hattori N. Pseudo-autosomal dominant inheritance of PARK2: two families with parkin gene mutations. J Neurol Sci. 2003;207: 11–17.
9. Mitsui J, Takahashi Y, Goto J, et al. Mechanisms of genomic instabilities underlying two common fragile-site-associated loci, PARK2 and DMD, in germ cell and cancer cell lines. Am J Hum Genet. 2010;87:75–89.
10. Cesari R, Martin ES, Calin GA, et al. Parkin, a gene implicated in autosomal recessive juvenile parkinsonism, is a candidate tumor suppressor gene on chromosome 6q25-q27. Proc Natl Acad Sci U S A. 2003;100:5956–5961.
11. Marder KS, Tang MX, Mejia-Santana H, et al. Predictors of parkin mutations in early-onset Parkinson disease: the consortium on risk for early-onset Parkinson disease study. Arch Neurol. 2010;67: 731–738.
12. Abou-Sleiman PM, Muqit MM, McDonald NQ, et al. A heterozygous effect for PINK1 mutations in Parkinson's disease? Ann Neurol. 2006;60:414–419.
13. Klein C, Lohmann-Hedrich K, Rogaeva E, Schlossmacher MG, Lang AE. Deciphering the role of heterozygous mutations in genes associated with parkinsonism. Lancet Neurol. 2007;6:652–662.
14. Aten E, White SJ, Kalf ME, et al. Methods to detect CNVs in the human genome. Cytogenet Genome Res. 2008;123:313–321.
15. Blauw HM, Veldink JH, van Es MA, et al. Copy-number variation in sporadic amyotrophic lateral sclerosis: a genome-wide screen. Lancet Neurol. 2008;7:319–326.
16. Tam GW, Redon R, Carter NP, Grant SG. The role of DNA copy number variation in schizophrenia. Biol Psychiatry. 2009;66: 1005–1012.
17. Singleton AB, Farrer M, Johnson J, et al. alpha-Synuclein locus triplication causes Parkinson's disease. Science. 2003;302:841.
18. Li Y, Tomiyama H, Sato K, et al. Clinicogenetic study of PINK1 mutations in autosomal recessive early-onset parkinsonism. Neurology. 2005;64:1955–1957.
19. Fuchs J, Nilsson C, Kachergus J, et al. Phenotypic variation in a large Swedish pedigree due to SNCA duplication and triplication. Neurology. 2007;68:916–922.

Imaizumi et al. Molecular Brain 2012, 5:35
http://www.molecularbrain.com/content/5/1/35

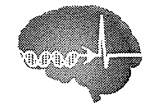

Molecular Brain

RESEARCH Open Access

Mitochondrial dysfunction associated with increased oxidative stress and α-synuclein accumulation in PARK2 iPSC-derived neurons and postmortem brain tissue

Yoichi Imaizumi[1], Yohei Okada[1,2], Wado Akamatsu[1], Masato Koike[3], Naoko Kuzumaki[1], Hideki Hayakawa[4], Tomoko Nihira[4], Tetsuro Kobayashi[5], Manabu Ohyama[5], Shigeto Sato[6], Masashi Takanashi[6], Manabu Funayama[6,7], Akiyoshi Hirayama[8], Tomoyoshi Soga[8], Takako Hishiki[9], Makoto Suematsu[9], Takuya Yagi[10], Daisuke Ito[10], Arifumi Kosakai[10], Kozo Hayashi[11], Masanobu Shouji[11], Atsushi Nakanishi[11], Norihiro Suzuki[10], Yoshikuni Mizuno[12], Noboru Mizushima[13], Masayuki Amagai[5], Yasuo Uchiyama[3], Hideki Mochizuki[4,14], Nobutaka Hattori[6,7] and Hideyuki Okano[1*]

Abstract

Background: Parkinson's disease (PD) is a neurodegenerative disease characterized by selective degeneration of dopaminergic neurons in the substantia nigra (SN). The familial form of PD, PARK2, is caused by mutations in the *parkin* gene. *parkin*-knockout mouse models show some abnormalities, but they do not fully recapitulate the pathophysiology of human PARK2.

Results: Here, we generated induced pluripotent stem cells (iPSCs) from two PARK2 patients. PARK2 iPSC-derived neurons showed increased oxidative stress and enhanced activity of the nuclear factor erythroid 2-related factor 2 (Nrf2) pathway. iPSC-derived neurons, but not fibroblasts or iPSCs, exhibited abnormal mitochondrial morphology and impaired mitochondrial homeostasis. Although PARK2 patients rarely exhibit Lewy body (LB) formation with an accumulation of α-synuclein, α-synuclein accumulation was observed in the postmortem brain of one of the donor patients. This accumulation was also seen in the iPSC-derived neurons in the same patient.

Conclusions: Thus, pathogenic changes in the brain of a PARK2 patient were recapitulated using iPSC technology. These novel findings reveal mechanistic insights into the onset of PARK2 and identify novel targets for drug screening and potential modified therapies for PD.

Keywords: Induced pluripotent stem cells, Parkinson's disease, Parkin, Oxidative stress, Mitochondria, α-synuclein

Background

Parkin is a causative gene of autosomal recessive juvenile Parkinson's disease (PARK2). It encodes a component of an E3 ubiquitin ligase involved in mitochondrial homeostasis [1-5]. *Parkin* deficiency is thought to result in aberrant ubiquitination and compromised mitochondrial integrity, leading to neuronal dysfunction and degeneration. Several PARK2 mouse models exist, but they do not replicate all of the pathogenic changes seen in human PARK2 neurons; thus, these models do not fully account for the molecular mechanisms of PD [6-9]. A recent report demonstrated that there is a defect in dopamine (DA) utilization in PARK2 induced pluripotent stem cell (iPSC)-derived neurons [10]. However, it is not known whether neuronal homeostasis is disrupted in PARK2 patients. Furthermore, studies have yet to demonstrate whether the phenotype of PD-specific iPSC-derived neurons recapitulates the *in vivo* phenotype of the corresponding cell donor. To address these questions, we generated iPSCs from two PARK2 patients

* Correspondence: hidokano@a2.keio.jp
[1]Department of Physiology, Keio University School of Medicine, 35 Shinanomachi, Shinjuku-ku, Tokyo 160-8582, Japan
Full list of author information is available at the end of the article

(PA and PB) [11]. In PARK2 iPSC-derived neurons, but not PARK2 fibroblasts or iPSCs, abnormal mitochondrial morphology and aberrant tubulovesicular structures adjacent to the Golgi were observed, as was increased oxidative stress. Although α-synuclein accumulation and Lewy body (LB) formation are very rare in PARK2 patients [1,12,13], we observed pathological changes and prominent LB formation, including the accumulation of α-synuclein, in postmortem brain tissue from one of the donor patients (PA). However, we obtained autopsied brain tissue from the father of donor PB, who carried the same *parkin* deletion as PB, and observed no evidence of LB formation or α-synuclein-positive cells. Consistent with these observations in postmortem brain tissue, increased α-synuclein accumulation was clearly observed in PA iPSC-derived neurons *in vitro,* but not in PB iPCS-derived neurons. These results are the first demonstration of pathogenic changes in the brain of a PARK2 patient that were recapitulated using iPSC technology. Our findings also provide mechanistic insights into PARK2 pathophysiology.

Results & discussion

Generation of PARK2 iPSCs

iPSCs were generated from dermal fibroblasts isolated from two PARK2 patients carrying *parkin* mutations and two control subjects using retroviruses carrying *Oct4, Sox2, Klf4,* and *c-Myc* to reprogram the cells as previously described [14,15]. The PARK2 patients were a 71-year-old female (PA) with a homozygous deletion of *parkin* exons 2–4 and a 50-year-old male (PB) with a homozygous deletion of exons 6 and 7 (Table 1 and Additional file 1A and B). Patient PA died 1 year after enrollment in the study at the age of 72. A previously-established human iPSC clone from control subject A, 201B7 (B7), was also used [15]. In addition, the following human embryonic stem cell (hESC)-like iPSC clones were selected for detailed analysis: three controls (B7 and YA9 from control A, and WD39 from control B), three from patient PA (PA1, PA9 and PA22), and four from patient PB (PB1, PB2, PB18 and PB20) (Figure 1A and Additional file 2A and B).

The PARK2 iPSCs expressed pluripotent hESC markers (Figure 1A and Additional file 2A-C) and formed teratomas containing all three germ layers (Additional file 2D).

Table 1 PA and PB patient information

	PA patient	PB patient
Race	Japanese	Japanese
Age	72 y/o	50 y/o
Sex	Female	Male
Age of onset	62 y/o	28 y/o
Mutation of *parkin*	Exon 2–4 homozygous deletions	Exon 6, 7 homozygous deletions

All of the retroviral transgenes were silenced in each clone (Additional file 2E). The iPSCs derived from PA and PB retained the corresponding homozygous *parkin* deletions and exhibited genomic stability (Figure 1B-D; Additional file 3A and B; and Table 1). All of the clones differentiated into neurons, including tyrosine hydroxylase (TH)-positive neurons, through a process of embryoid body and neurosphere formation (Figure 1A). Thus, all of the lines were successfully reprogrammed into a pluripotent state and were suitable for further analysis.

Increased oxidative stress accompanied by activation of the Nrf2 pathway in PARK2 iPSC-derived neurons

Because increased levels of oxidative stress have been documented in other PD models [7,10,16,17], we examined oxidative metabolism in the iPSC clones by measuring the cellular levels of reduced glutathione (GSH). GSH reacts with reactive oxygen species (ROS) and is catalyzed by glutathione S-transferase[18]. Consistent with previous results from patient-derived cells [16], the levels of GSH in PARK2 iPSC-derived neurospheres were significantly lower than those in control iPSC-derived neurospheres (Figure 2A). We also examined ROS production using 2', 7'-dichlorodihydrofluorescin (DCF) fluorescence to measure the levels of intracellular oxidants. The DCF fluorescence intensity in the PARK2 iPSC-derived neurons was significantly higher than that in control iPSC-derived neurons (Figure 2B and C), which indicated an increased level of oxidative stress. A recent study showed that, in PARK2 iPSC-derived neurons, monoamine oxidase (MAO)-A and -B levels and oxidative stress levels are increased, as is spontaneous DA release [10]. Here, we found no significant differences in MAO-A and -B expression levels between PARK2 and control neurons (Additional file 4A and B).

The Nrf2 pathway plays a cytoprotective role under conditions of ROS accumulation. Recent studies show that activation of the Nrf2 pathway reduces oxidative stress and provides partial protection from MPTP-mediated neurotoxicity[19]. Elevated Nrf2 expression was observed in the postmortem brain of a PD patient [20]. These data suggest a putative link between the Nrf2 pathway and PD, and prompted a closer investigation of this signaling pathway in control and PARK2 iPSC-derived neurons [19-21]. The expression of Nrf2 pathway proteins, such as Nrf2 and NADH quinone oxidoreductase (NQO1), was significantly increased in PARK2 iPSC-derived neurons (Figure 2D and E). These data are in line with previous reports [19-21], and suggest that the Nrf2 cytoprotective pathway may be activated in PARK2 iPSC-derived neurons to prevent further damage from oxidative stress. Taken together, these data demonstrated an increased level of

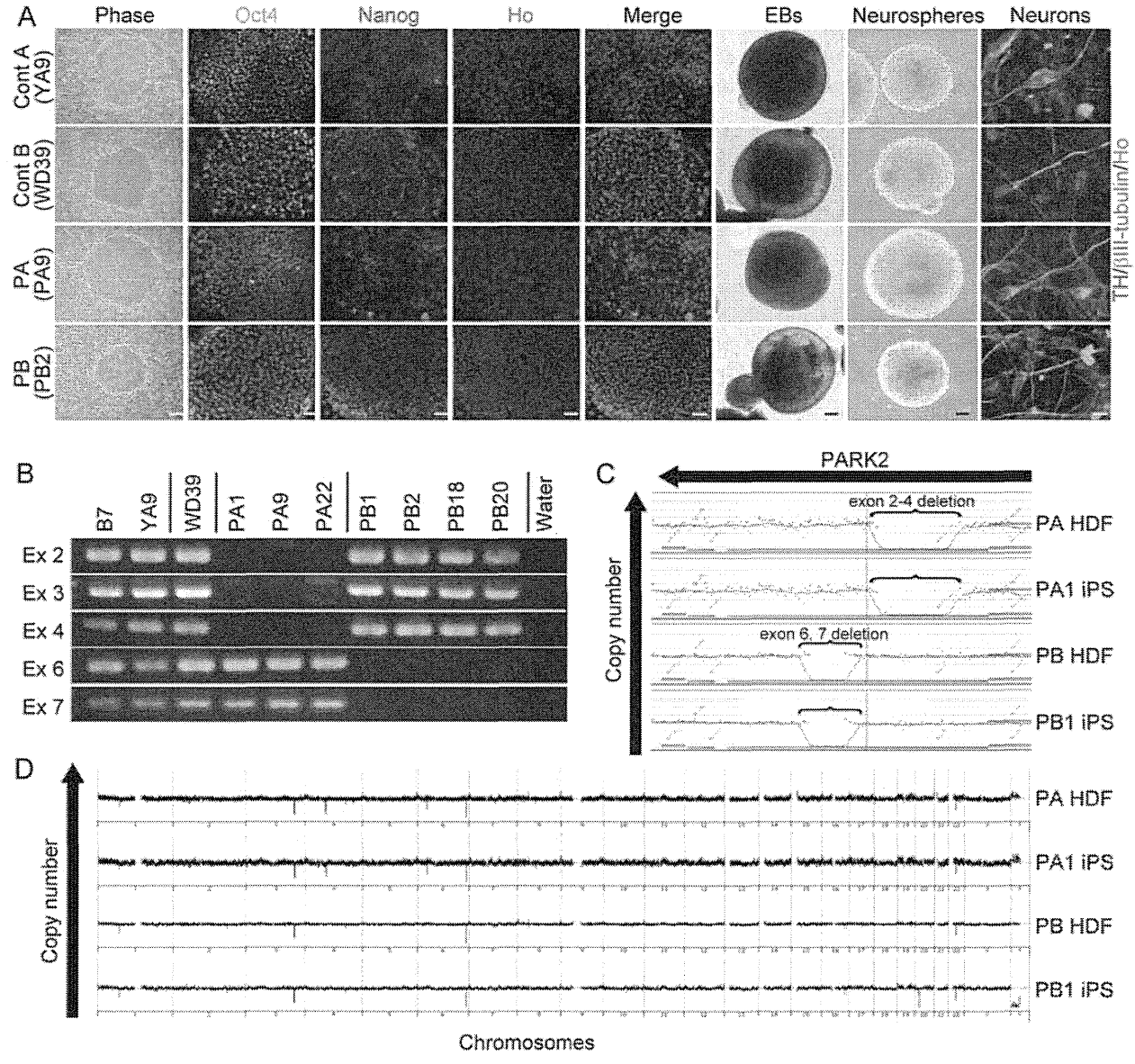

Figure 1 Generation of PARK2 iPSCs. (**A**) iPSCs derived from control and PARK2 subjects, embryoid bodies (EBs), neurospheres (NSs), and neurons. *Left three rows*: iPSCs from Control A (YA9), Control B (WD39), PA (PA9), and PB (PB2) were immunopositive for the pluripotency markers Oct4 (green) and Nanog (red). *Right three rows:* Differentiation of iPSCs into tyrosine hydroxylase (TH)-positive (red) neurons via EB and NS formation. Scale bars: Phase contrast, 400 μm; Nanog and Oct4 immunostaining, 100 μm; EBs, 25 μm; NSs, 50 μm; neurons, 10 μm. (**B**) Deletion of exons 2–4 in clones PA1, 9 and 22; and of exons 6 and 7 in clones PB1, 2, 18, and 20 was confirmed. (**C**) Exons 2–4 were deleted in human dermal fibroblasts (HDFs) from PA and in PA1 iPSC lines. Exons 6 and 7 were deleted in HDFs from PB and PB1 iPSC lines. (**D**) Copy number profiles of whole chromosomes in PARK2 HDFs and iPSCs were assessed by comparative genomic hybridization (CGH) microarray analysis; there was no evidence that genomic aberrations were introduced during the process of establishing PARK2 iPSCs.

oxidative stress accompanied by activation of the Nrf2 pathway in PARK2 neurons.

Abnormal mitochondrial morphology and impaired mitochondrial turnover in PARK2 iPSC-derived neurons

Increased oxidative stress (which affects anti-oxidant defense systems) and mitochondrial dysfunction are implicated in the pathogenesis of PD [1,13,21-23]. Furthermore, ROS accumulation causes both oxidative damage and mitochondrial dysfunction in the substantia nigra (SN) of *parkin*-deficient mice [7]. However, the exact mechanism of mitochondrial pathogenesis associated with PARK2 is controversial. For example, while *Drosophila parkin* mutants show abnormal mitochondrial morphology, *parkin*-knockout mice do not [7,24]. In addition, while a greater degree of mitochondrial branching is observed in

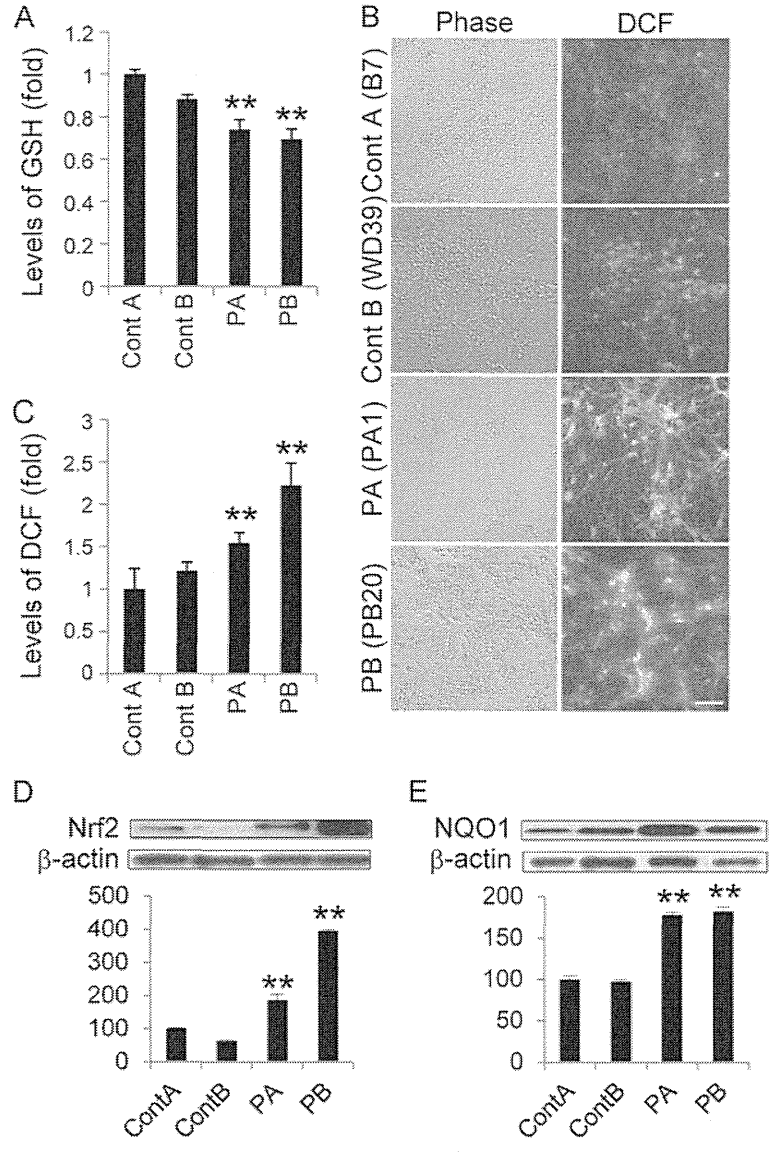

Figure 2 Increased oxidative stress accompanied by activation of the Nrf2 pathway in PARK2 iPSC-derived neurons. (**A**) GSH levels were significantly reduced in PARK2 (PA1, 9 and 22, and PB2, 18 and 20) iPSC-derived neurospheres compared with those in control A (YA9) and B (WD39) neurospheres. (**B, C**) DCF fluorescence intensity in PARK2 (PA1, 9 and 22, and PB2 and 20) iPSC-derived neurons was significantly higher than that in control A (B7) and B (WD39) neurons. (**D, E**) Immunoblot analysis of Nrf2 and NQO1 levels in iPSC-derived neurons from PA and PB. Expression of Nrf2 and NQO1 in PARK2 (PA9 and PB2) iPSC-derived neurons was significantly higher than that in control A (YA9) and B (WD39) neurons. Relative protein abundance was normalized to β-actin. ** indicates $P < 0.01$ (Mann–Whitney *U*-test). Data represent the mean and SEM of at least three experiments for each group.

fibroblasts derived from PARK2 patients, the detailed morphology of the mitochondria in these cells has not been characterized [25]. To investigate these mitochondrial abnormalities in more depth, we performed a detailed morphological analysis of mitochondria in PARK2 iPSC-derived neurons using electron microscopy. Mitochondria in PARK2 neurons from both patients showed a highly electron-dense matrix and swollen mitochondrial cristae within the inner mitochondrial membrane (IMM) (Figure 3A, black arrowheads). The perikaryal volume density of the abnormal mitochondria was significantly increased in PA and PB iPSC-derived neurons relative to control clones (Figure 3B). Furthermore, the density of normal mitochondria decreased (Figure 3B). Importantly, both abnormal and normal mitochondria were observed in PARK2 neurons (Figure 3A, white arrowheads). Abnormal mitochondria were observed in 87.8% of iPSC-derived neurons from PA, and 79.5% of iPSC-derived neurons from PB. These data indicated that abnormal mitochondrial morphology was a feature of most PARK2 iPSC-derived

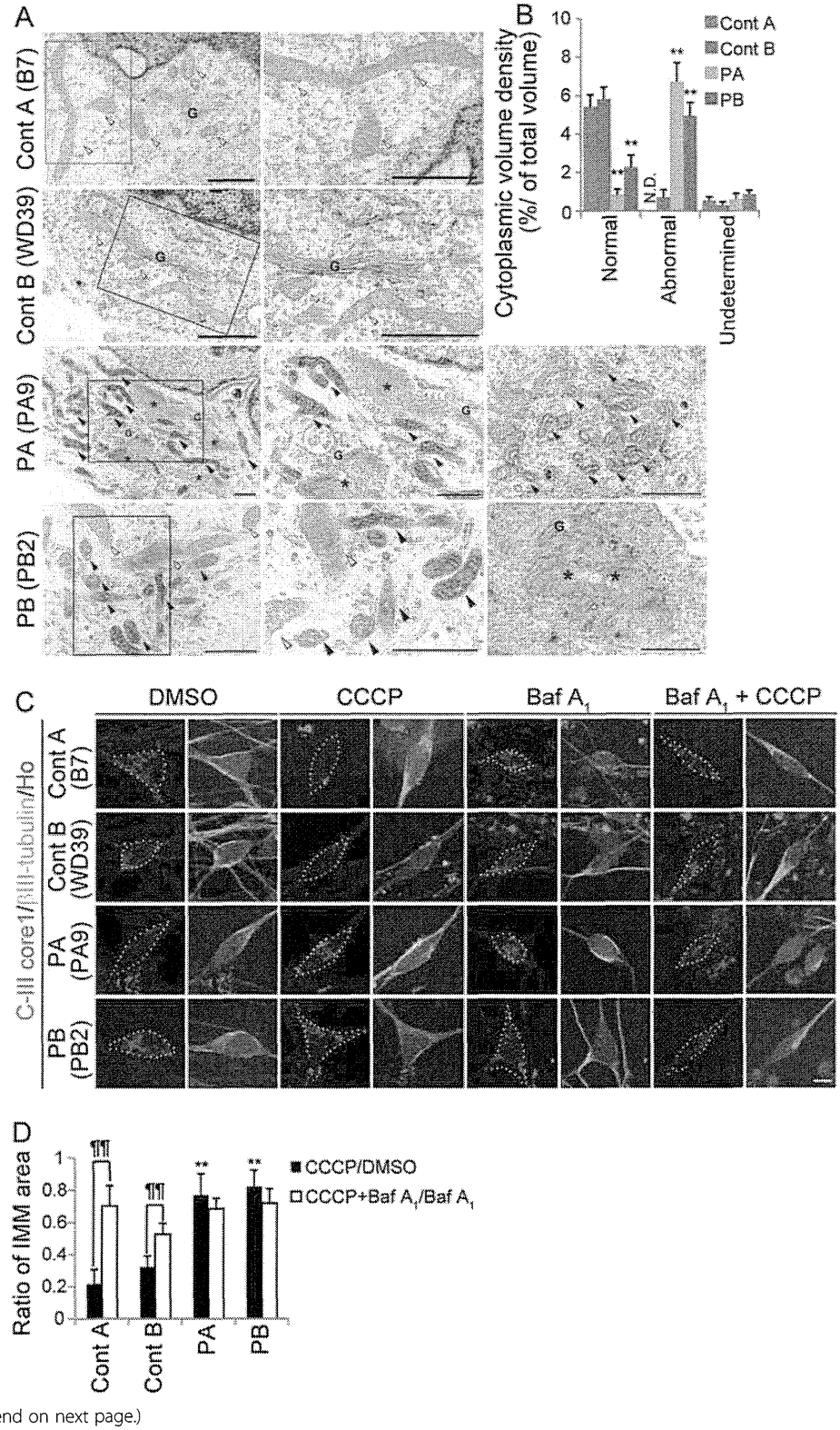

Figure 3 (See legend on next page.)

(See figure on previous page.)
Figure 3 Dysregulation of mitochondrial homeostasis in PARK2 iPSC-derived neurons. (**A**) Electron micrographs of control A (B7), control B (WD39) and PARK2 (PA9 and PB2) iPSC-derived neurons. Boxed areas are shown in the enlarged images to the right. Control mitochondria showed a characteristically long, cylindrical profile with well-organized cristae, and the electron density of the matrix was relatively low (white arrowheads). By contrast, increased electron density of the matrix was evident in PARK2 mitochondria (black arrowheads), and the cristae often appeared swollen. As shown in PB2, some of the neurons contained both morphologically intact (white arrowheads) and abnormal (black arrowheads) mitochondria. Furthermore, abnormal tubulovesicular structures (asterisks) were observed adjacent to the Golgi cisternae (G). (**B**) The relative perikaryal volume of the abnormal mitochondria was significantly increased, and that of the normal mitochondria was decreased, in PARK2 neurons compared with control neurons. (**C**) Double labeling for the IMM marker, ComplexIII corel (CIII-Core I; magenta) and βIII-tubulin (green) of control A (B7), control B (WD39) and PARK2 (PA9 and PB2) iPSC-derived neurons. The volume of the IMM area was reduced in control neurons treated with CCCP, but not in PARK2 neurons treated with CCCP. Administration of Baf A_1 rescued the CCCP-induced phenotype in control neurons. (**D**) The CCCP/DMSO ratio in control A (B7 and YA9) and B (WD39) neurons was reduced after CCCP treatment. This reduction was not observed in PARK2 (PA1, 9 and 22, and PB2 and 20) iPSC-derived neurons (black bars indicate CCCP/DMSO ratio; white bars indicate Baf A_1+CCCP/Baf A_1 ratio). ** indicates $P < 0.01$ compared with the control; ¶¶ indicates $P < 0.01$ when comparing the black and white bars (Mann–Whitney *U*-test). At least three experiments were performed for each group, with 5–36 cells quantified per experiment. Scale bars: a, 1 μm; c, 10 μm. Error bars represent the SEM. N.D., not detected.

neurons from these patients. In addition, abnormal tubulovesicular structures were observed adjacent to the Golgi cisternae in PARK2 iPSC-derived neurons (Figure 3A). These abnormal mitochondrial and tubulovesicular structures were not observed in PARK2 fibroblasts or in undifferentiated iPSCs (Additional file 5A and B). These histological abnormalities represent novel PARK2-related neuronal pathologies.

PARKIN is involved in the mitochondrial fission/fusion system and is recruited to depolarized mitochondria to promote mitophagy [5,26-29]. In iPSC-derived neurons containing a mutation in PINK1 (a protein kinase upstream of PARKIN), PARKIN is not recruited appropriately to mitochondria [30]. We hypothesized that PARKIN-deficient human neurons would show aberrant removal of depolarized mitochondria. To examine the turnover of damaged mitochondria, we treated iPSC-derived neurons with carbonyl cyanide m-chlorophenyl hydrazine (CCCP), which triggers the loss of mitochondrial membrane potential and results in the removal of damaged mitochondria. The intensity of TMRE, a mitochondrial membrane potential-dependent dye, clearly decreased in both control and PARK2 iPSC-derived neurons treated with CCCP, which indicated a reduced mitochondrial membrane potential in both sets of neurons (Additional file 6). To determine the extent to which the damaged mitochondria were eliminated, we measured the area of the IMM after CCCP treatment. Compared with untreated cells, there was a dramatic loss of IMM area in the treated control neurons, but not in the treated PARK2 neurons (Figure 3C, left four columns; Figure 3D, black bars). To assess whether lysosomes were involved in the CCCP-induced elimination of mitochondria, we treated cells with Bafilomycin (Baf) A_1, an inhibitor of the vacuolar type H(+)-ATPase. Baf A_1 attenuated the CCCP-dependent reduction in the IMM area in control neurons (Figure 3C, right four columns; Figure 3D, white bars). To confirm that the abnormal turnover of damaged mitochondria was characteristic of neuronal cells, PARK2 fibroblasts and undifferentiated iPSCs were treated with CCCP. CCCP-treated PARK2 fibroblasts and undifferentiated iPSCs exhibited the same mitochondrial dynamics as CCCP-treated control cells (Additional file 5C-E). Together, these data indicated aberrant degradation of mitochondria damaged by CCCP treatment in PARK2 iPSC-derived neurons.

These results support a recently proposed working model for PD, in which damaged mitochondria accumulate due to a disruption in PARKIN-mediated mitochondrial quality control [28]. The electron microscopy data, which showed a mixture of abnormal and normal mitochondria, indicated that PARKIN-mediated mitochondrial quality control is compromised, even in young PARK2 iPSC-derived neurons. In these cells, residual normal mitochondria may have compensated for the damaged ones. Thus, while our findings suggest that the PARKIN-dependent mechanisms that regulate mitochondrial homeostasis are disrupted in PARK2 cells, further detailed analyses are required to fully understand the mechanism underlying this disruption and the implications for PD.

Patient-specific accumulation of α-synuclein in PARK2 iPSC-derived neurons and its correlation with LB formation

LBs are pathological neuronal inclusions composed principally of α-synuclein. They are typically associated with PD and certain forms of dementia [1,13,31]. Although LBs are generally thought to be absent from PARK2 patients [1,13,31], rare cases of LB formation in the brains of PARK2 patients have been reported recently [12,32,33]. The PARKIN protein co-localizes with LBs in some patients with sporadic PD [34], and a functional interaction between PARKIN and α-synuclein is indicated by both *in vitro* and *in vivo* findings [35-37]. These results suggest that PARKIN-pathway may contribute to LB formation in PD patients.

We were able to conduct a histopathological analysis of postmortem brain tissue from patient PA. Hematoxylin and eosin staining of the SN revealed low levels of brown-black

melanin pigment compared with healthy SN tissue (Figure 4A and A'). Surprisingly, LBs accumulated in the SN and other areas of the brain in patient PA (Figure 4B and Table 2). Furthermore, α-synuclein and pα-synuclein immunoreactive puncta and neurites were observed in the areas where LBs were present (Figure 4B). TH/pα-synuclein double-positive neurons were also detected in the SN (Figure 4C). Of note, α-synuclein-positive/TH-negative or pα-synuclein-positive/TH-negative neurons in the SN and other areas of the brain tissue from patient PA's brain were observed (Table 2). These data suggested that α-synuclein accumulated not only in TH+ neurons, but also in other types of neurons. Postmortem tissue from the brain of the father of patient PB was also examined. The father carried a homozygous deletion of exons 6 and 7 of the *parkin* gene (Figure 1B, Additional file 1B and 7A), similar to patient PB. There was no evidence of LBs or α-synuclein-positive neurons in the autopsied brain tissue of the father (Figure 4D). Thus, since the genetic background of patient PB and his father are likely to be very close (Additional file 1B and 7A), these results are probably reflective of a specific phenotype of patient PB, which was different from that in patient PA (Figure 4A-D).

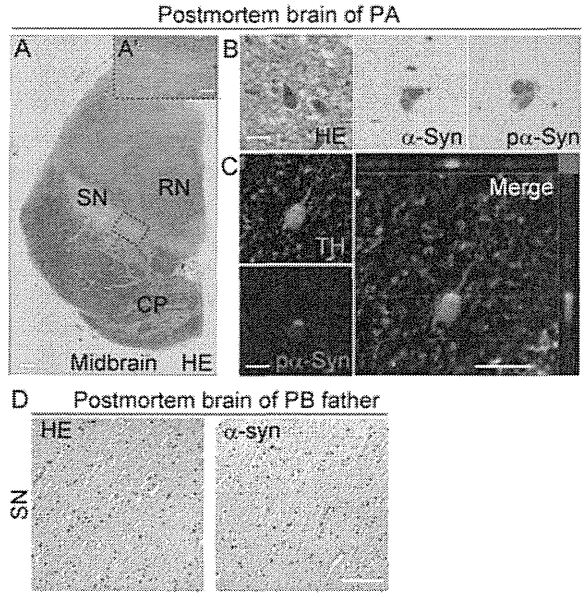

Figure 4 Accumulation of LBs in the postmortem brain of patient PA. (**A**–**C**) Immunohistochemical staining of postmortem brain tissue from patient PA. (**A**) Low magnification image of a midbrain section stained with hematoxylin and eosin (H&E). (**A'**) High magnification image of the boxed area. Melanin levels were reduced in most of the substantia nigra (SN). (**B**) (Left) High magnification image of a midbrain section stained with H&E showing the presence of Lewy bodies (LBs) in the SN. (Middle and Right) α-synuclein-positive and pα-synuclein-positive cells in the SN. (**C**) Confocal microscopy image of a TH (green) and pα-synuclein (red) double-positive SN neuron and a projected merged image: pα-synuclein accumulated in the TH-positive neuron. (**D**) Melanin levels were reduced in most of the SN. No LBs or α-synuclein-positive neurons were observed in postmortem brain tissue from the father of patient PB. Scale bars: A, 1000 μm; A', 350 μm; B, C, 50 μm; D, 100 μm.

To determine whether iPSC-derived neurons recapitulated the *in vivo* phenotypes of the corresponding cell donors, we next examined α-synuclein accumulation in PARK2 iPSC-derived neurons. To rule out the possibility that α-synuclein expression in undifferentiated PARK2 iPSCs was increased by multiplication of the *SNCA* gene, genomic aberrations acquired during the process of iPSC establishment, or by repeated passage of the cells, the *SNCA* gene copy number in iPSCs was quantified by genomic qPCR. A comparison with control iPSCs showed that iPSCs from both PA and PB carried the normal number of *SNCA* gene copies (Additional file 8A). Moreover, immunostaining for α-synuclein did not reveal any increase or decrease in α-synuclein protein levels in PARK2 iPSCs (Additional file 8B). As a control for LB formation, we generated iPSC-derived neurons from a 106-year-old woman (designated Cent1-8), since previous work suggested that aging is a predisposing factor for LB formation in PD patients [31,38]. Since α-synuclein was also expressed in non-neural cells, triple labeling for α-synuclein, βIII-tubulin, and TH was performed to ensure that only neurons were examined (Figure 5A, asterisks). The proportion of α-synuclein-positive iPSC-derived neurons that were also positive for βIII-tubulin from PB was similar to that in the controls (including Cent1-8); however, the proportion was significantly higher in PA. These results were consistent with the *in vivo* phenotypes of the cell donors based on analysis of postmortem brain tissue (1629, 357, 805, 3747, and 4330 iPSC-derived βIII-tubulin+ neurons in control A, control B, Cent1-8, PA and PB respectively; Figure 5A-C, arrows and arrowheads). Thus, the increase in α-synuclein expression levels seen in PARK2 iPSC-derived neurons

Table 2 LB type pathology in PA patient's postmortem brain

Brain area		LB type pathology
Brainstem lesion	IX-X	+++
	LC	+++
	SN	++
Basal forebrain/Limbic	nbM	++
	Amy	++
	Ent	+
	Cing	+
Neocortical	T	-
	F	-
	P	-

IX-X, motor cranial nerves IX-X; *LC*, Locus Coeruleus; *SN*, Substantia Nigra; *nbM*, nucleus basal of Meynert; Amy, Amygdala; Ent, Entorhinal cortex; T, Temporal lobe; F, Frontal lobe; P, Parietal lobe.

cannot be attributed solely to the effects of aging, but associated with the disease phenotype.

The obvious LB-formation was observed in the postmortem brain of PA patient, who showed a late onset at 61 years, corresponding to the enhanced α-synuclein accumulation in the iPSC-derived neurons from the same patient. Thus, it is likely that early-stage LB formation was recapitulated *in vitro* in iPSC-derived neurons. Furthermore, the present findings are consistent with recent work by several groups, which suggest that the age of onset of PARK2 in patients with LB formation (41 on average) is later than in patients without LB formation (below 40) [12,32,33]. The earlier onset in patient PB (at 28 years) than in PA (at 61 years) would be consistent with the finding of lower α-synuclein accumulation in PB iPSC-derived neurons compared with PA iPSC-derived neurons. On the other hand, and in contrast to the observations of brain tissue from PA, analysis of brain tissue from the father of patient PB, in whom the onset of PD was 39 years of age, revealed no evidence of LB formation (Figure 4D). Importantly, PA iPSC-derived neurons showed significantly more α-synuclein accumulation than PB iPSC-derived neurons (Figure 5A and C). These results suggest that the extent of α-synuclein accumulation is an important factor in LB formation. Then, how can we explain the difference of α-synuclein accumulation between PA and PB patients-derived neuronal cells? It is possible that PA is a rare example of PARK2 complicated by sporadic PD. Although both PA and PB iPSCs showed a normal *SNCA* gene copy number, it is possible that PA-derived cells acquired an unknown gene mutation relating to LB formation. Thus, we cannot rule out the possibility that other factors may affect LB formation in PARK2 patients. Further analyses will be required to identify these putative factors. Although iPSC clones from sporadic and familial PD patients were recently established [17,30,39-42], this report is the first to demonstrate that the phenotype of PD-specific iPSC-derived neurons replicates the *in vivo* phenotype seen in postmortem brain tissue from the corresponding cell donor.

Conclusions

In summary, dysfunctional neuronal homeostasis (characterized by increased oxidative stress and activation of the Nrf2 pathway), impaired mitochondrial function, and increased α-synuclein accumulation were observed in PARK2 iPSC-derived neurons. These results indicate that PARK2-associated phenotypes may appear soon after, or possibly even before, the onset of PARK2. Detailed analyses of PARK2 iPSC-derived neurons, particularly mature neurons, to determine the time course of LB accumulation and synaptic dysfunction will be of great interest. Such analyses will further our understanding of the pathogenesis of PARK2 as well as sporadic PD. The ultimate goal is the development and application of novel preventative therapies for PD.

Materials & methods

Isolation of human skin fibroblasts and generation of iPSCs

For control A, human dermal fibroblasts (HDFs) from the facial dermis of a 36-year-old Caucasian female (Cell Applications Inc.) were used to establish iPSCs (201B7; Passage 20–29, YA9; Passage 15–24). The 201B7 iPSCs were kindly provided by Dr. Yamanaka [15]. A skin-punch biopsy from a healthy 16-year-old Japanese female obtained after written informed consent (Keio University School of Medicine) was used to generate the control B iPSCs (WD39; Passage 8–17). PA iPSCs (PA1, 9, and 22; Passage 10–19) and PB iPSCs (PB1, 2, 18, and 20; Passage 8–17) were generated from a 71-year-old Japanese female patient and a 50-year-old Japanese male patient, respectively, using the same methods used to generate control B iPSCs. The maintenance of HDFs, lentiviral production, retroviral production, infection, stem cell culture and characterization, and teratoma formation were performed as described previously [14,15]. All of the experimental procedures for skin biopsy and iPS production were approved by the Keio University School of Medicine Ethics committee (Approval Number: 20-16-18) and Juntendo University School of Medicine Ethics committee (Approval Number: 2012068). hESCs (KhES-1; Passage 29–38 (kindly provided by Dr. Norio Nakatsuji) were cultured on feeder cells in iPS culture media [43].

In vitro differentiation of human iPSCs

Neural differentiation of iPSCs was performed as previously described [44] with slight modifications (Okada et al., manuscript in preparation). Briefly, iPSC colonies were detached from feeder layers and cultured in suspension as EBs for about 30 days in bacteriological dishes. EBs were then enzymatically dissociated into single cells and the dissociated cells cultured in suspension in serum-free media (MHM) [44] for 10 to 14 days to allow the formation of neurospheres. Neurospheres were passaged repeatedly by dissociation into single cells followed by culture in the same manner. Typically, neurospheres between passages 3 and 8 were used for analysis. For terminal differentiation, dissociated or undissociated neurospheres were allowed to adhere to poly-L-ornithine- and fibronectin-coated coverslips and cultured for 10 days.

Immunocytochemical analysis of iPSCs and neurons

For immunocytochemical analysis, cells were fixed with phosphate buffered saline (PBS) containing 4% paraformaldehyde (PFA) for 30 min at room temperature (RT). The cells were analyzed by immunofluorescence staining using antibodies to the following proteins: β-III-tubulin (1:1000,